Applied Science, Computing and Energy, 2026, 4(3), 474-504

Unravelling Gold Mineralization Pathways in a Pan-African Basement Terrane: Integrated Evidence from Geochemistry, Mineral Inclusions and Gold-Grain Chemistry

Onasanwo Anthony Adesoji, Benjamin Odey Omang, Michael Ekuru Omeka. *and* Akumbom Vishiti

Received: 18 February 2026/Accepted: 01 May 2026/Published: 10 May 2026

Abstract: *Even with growing evidence of considerable mineral potential in southeastern Nigeria, a key challenge is understanding the origin and metallogenic evolution of gold mineralization in the Obudu Plateau–Boki–Oban Massif of the southeastern Nigerian Basement Complex. This study combines stream-sediment geochemistry, mineralogical characterization, multivariate statistical analysis, and gold-grain microchemistry to establish the genesis of gold and associated mineralization in the region. Trace elements in representative samples of stream sediment, soil, and rock were analyzed by inductively coupled plasma–mass spectrometry (ICP–MS), and gold grains and associated mineral inclusions were examined by scanning electron microscopy (SEM–EDS), X-ray diffraction (XRD), and electron probe microanalysis (EMPA). Geochemical results indicate substantially elevated Au levels (up to 0.56 ppm), along with anomalous As, Sb, Pb, Sn, Nb, Y, and rare-earth elements, suggesting contributions from hydrothermal and evolved granitic mineralizing systems. Principal Component Analysis revealed distinct Au–As–Sb and Nb–Sn–REE associations, indicating different metallogenetic processes. Gold grains are mostly sub-rounded, with Ag-depleted core-rim textures suggesting proximal transport and supergene modification. EMPA analyses show fineness values from 936 to 1000 in Oban and from 990 to 996 in Besenge. Cassiterite inclusions in the Oban gold grains, with minor Cu enrichment and variable fineness, indicate derivation from a granite-related magmatic-hydrothermal Au-Sn system. In contrast, the euhedral LREE-rich, low-Th monazite inclusions and the consistently high-fineness gold of Besenge are typical for structurally controlled orogenic metamorphic-hydrothermal mineralization. Integration of geochemical, mineralogical and microchemical data indicates co-occurrence of granite-related Au–Sn and orogenic gold systems in the study area. These findings provide the first integrated metallogenic framework for the Obudu Plateau–Boki–Oban Massif and identify priority exploration targets for gold, tin, niobium and rare-metal mineralization in southeastern Nigeria.*

Keywords: *Gold-grain microchemistry; Metallogenic evolution; Granite-related Au–Sn mineralization; Orogenic gold deposits; Obudu Plateau–Oban Massif; Pan-African Basement Complex*

Onasanwo Anthony Adesoji
Department of Geology, University of Calabar, P.M.B. 1115, Calabar, Cross River State, Nigeria.
Email: adsojt@gmail.com

Benjamin Odey Omang*
Department of Geology, University of Calabar, P.M.B. 1115, Calabar, Cross River State, Nigeria.
Email: benjaminomang@unical.edu.ng
https://orcid.org/0000-0001-9196-3109

Michael Ekuru Omeka
Department of Geology, University of Calabar, P.M.B. 1115, Calabar, Cross River State, Nigeria.
Email: omeka.ekuru@unical.edu.ng
https://orcid.org/0000-0003-0405-8616

Akumbom Vishiti
Department of Civil Engineering, University Institute of Technology (IUT), University of Douala, P.O. Box 8698, Douala, Littoral Region, Cameroon.
Email: akumbom@gmail.com

1.0 Introduction

Gold remains one of the most economically important mineral commodities in the world due to its strategic role in monetary reserves, advanced technologies, jewellery manufacturing, and new green-energy applications. Exploration for new deposits has increased due to global demand for gold, particularly in Precambrian cratons and Pan-African mobile belts, which host many world-class gold provinces (Goldfarb & Groves, 2015). Advances in mineral exploration in recent decades have demonstrated that successful discovery strategies increasingly rely on integrating geochemical, mineralogical, and microchemical datasets to link surficial geochemical anomalies to buried mineralization systems. Accordingly, modern metallogenic research has begun to shift away from traditional reconnaissance geochemistry towards multidisciplinary approaches that combine regional geochemical surveys with detailed characterisation of ore minerals and placer gold grains.

One of the least-explored but potentially important metallogenic provinces in West Africa is the Pan-African Basement Complex of Nigeria. The schist belts of northwestern and southwestern Nigeria have received considerable attention for their economic gold occurrences, but little is known about the metallogenic evolution and gold potential of southeastern Nigeria. The Obudu Plateau–Boki–Oban Massif is a particularly significant component of the Pan-African mobile belt, as it forms part of the transboundary Nigeria–Cameroon Basement Complex and exhibits an extensive history of magmatism, deformation, metamorphism, and hydrothermal activity associated with the Neoproterozoic Pan-African Orogeny. Regional geological investigations revealed widespread granitoid intrusions, migmatitic gneisses, amphibolites, pegmatites, quartz veins and large structural lineaments indicating favourable conditions for the development of hydrothermal mineral systems (Ekwueme & Kröner, 2006).

Historical mineral exploration in southeastern Nigeria has mainly focused on geological mapping, stream-sediment reconnaissance, and artisanal gold occurrences. These studies have confirmed anomalous concentrations of gold, tin, niobium, rare-earth elements, and associated pathfinder elements, indicating multiple mineralizing systems in the basement terrain. Yet, even with growing recognition of the region's mineral potential, the genetic relationships among geochemical anomalies, ore minerals, and gold occurrences remain poorly constrained. As such, the origin, timing and metallogenic significance of mineralization in the Obudu–Oban basement province remain subjects of considerable uncertainty.

Stream-sediment geochemistry has long been regarded as one of the most effective exploration tools in tropical terrains, since sediments integrate geochemical signatures from large upstream catchments, providing a regional view of mineralization processes. Stream sediments from the Canadian Shield, the Fennoscandian Shield, the Amazonian Craton and the Central African Fold Belt have been shown to preserve diagnostic trace-element associations that can be used to identify concealed ore systems and define metallogenic provinces (McClenaghan, 2012). More recently, the application of high-resolution ICP-MS has greatly improved the sensitivity of stream-sediment investigations, enabling the simultaneous determination of major elements, trace elements, platinum group elements (PGEs), and rare earth elements (REEs). These datasets offer valuable information on provenance, weathering processes, hydrothermal alteration and ore-forming environments.

Regional geochemistry provides information on patterns of elemental dispersion, but generally does not provide sufficient detail to determine the precise nature of the primary mineralization source. There has therefore been an increasing emphasis on integrating

geochemical datasets with studies of ore minerals and gold grains. Gold grains are excellent exploration indicators because they retain the mineralogical and chemical signatures of their source deposits. The morphology of gold, alloy composition, fineness, and mineral inclusions have been used in previous studies in Australia, Canada, Finland, Cameroon, Tanzania, and Brazil to distinguish among orogenic, epithermal, intrusion-related, and granite-associated gold systems (Chapman *et al*., 2018; Chapman & Mortensen, 2006).). For example, in the Canadian Cordillera, detrital gold grain chemistry was shown to be a good discriminator among several deposit types within a single drainage basin, thereby increasing exploration targeting efficiency.

The advent of scanning electron microscopy (SEM), energy-dispersive spectroscopy (EDS), and electron probe microanalysis (EMPA) has further revolutionized gold exploration by enabling detailed characterization of gold grain microtextures and mineral inclusions. Chapman & Mortensen (2006) showed that mineral inclusions within placer gold grains provide direct evidence of ore-forming environments, as they are trapped during gold precipitation and shielded from subsequent weathering. Later studies from Cameroon, Tanzania and the Amazonian Craton have demonstrated that inclusions such as monazite, cassiterite, pyrite, arsenopyrite, zircon and rutile can provide important information on source lithology, hydrothermal conditions and metallogenic affinity. For example, the presence of cassiterite inclusions is a typical marker for granite-related hydrothermal Au–Sn systems, whereas monazite-bearing gold is often a signature of metamorphic-hydrothermal or orogenic gold settings.

Multivariate statistical techniques are also increasingly important in mineral exploration because modern geochemical datasets often contain dozens of interrelated variables that are difficult to interpret using univariate approaches alone. Principal Component Analysis (PCA) and similar techniques are often used to determine elemental associations, separate lithological controls from hydrothermal signatures, and identify geochemical processes associated with mineralization. PCA has been successfully used in the Arabian-Nubian Shield, the Central African Fold Belt, the Canadian Shield, and the West African Birimian terranes to separate ore-related element assemblages and elucidate hidden metallogenic processes not evident from conventional geochemical interpretation.

Although these methodological advances have been widely applied elsewhere, integrated studies that combine ICP–MS geochemistry, multivariate statistical modelling, SEM–EDS mineral characterization, and EMPA gold-grain microchemistry are very rare in the Nigerian Basement Complex. Previous work in southeastern Nigeria has mainly focused on regional geology, petrography, structural interpretation, or reconnaissance geochemical surveys, with few efforts to establish direct relationships between geochemical anomalies and ore-forming processes. Moreover, no previous study has integrated stream-sediment geochemistry, gold-grain chemistry, mineral inclusion analysis, tectonic discrimination and multivariate statistical modelling to build a metallogenic framework for the Obudu Plateau-Boki-Oban Massif.

This lack of knowledge has hindered the understanding of the origin of gold mineralization in the region and limited the development of effective exploration strategies. In particular, uncertainties persist regarding whether the reported gold occurrences are related to structurally controlled orogenic systems, granite-associated hydrothermal mineralization, or multiple overlapping metallogenic events. Relationships between gold, tin, rare-earth elements, platinum-group elements, and high-field-strength elements are similarly poorly constrained.

The present study attempts to fill these gaps by combining ICP–MS geochemistry of rocks, soils and stream sediments with SEM–EDS, XRD and EMPA investigations of gold grains and associated minerals. This study develops a comprehensive metallogenic model for the Obudu Plateau–Boki–Oban Massif through integrated application of multivariate statistical analysis, tectonic discrimination, mineralogical characterization, and gold-grain microchemistry.

The Objectives of the Study include to: (1) characterize the geochemical signatures of stream sediments using ICP–MS in order to identify elemental associations, pathfinder elements, and mineralization anomalies within the study area, (2) determine the morphology, alloy chemistry, fineness characteristics, and mineral inclusions of placer gold grains using SEM–EDS and Electron Probe Micro-Analysis (EMPA) and evaluate their implications for deposit genesis, (3) investigate the mineralogical composition and paragenetic relationships of ore-related minerals through integrated SEM, EDS, and XRD analyses, (4) evaluate the tectonic and metallogenic significance of major, trace, and rare-earth element distributions using multivariate statistical approaches and tectonic discrimination techniques, and (5) integrate geochemical, mineralogical, and gold-grain microchemical evidence in order to establish a genetic model for gold mineralization and identify priority exploration targets within the Obudu Plateau–Boki–Oban Massif.

The study is the first systematic evaluation of the genetic relationships between gold mineralization, granite-related Au–Sn systems, rare-metal enrichment and Pan-African tectonic evolution in southeastern Nigeria. Beyond its regional importance, this study exemplifies how combining regional geochemistry and gold-grain microchemistry can be a powerful approach to mineral exploration in tropical Precambrian terranes.

2.0 Study Area Description

2.1 Location and Accessibility.

The study was carried out in the Oban Massif and the Obudu Plateau. Both basement areas are located in Cross River State, southeastern Nigeria, and are western extensions of the Adamawa Plateau. The Oban Massif lies between 5°15′ and 5°45′ latitude and between 8°00′ and 8°20′ longitude. The Obudu Plateau is situated between 8°39′ and 9°29′ E longitude and between 6°00′ and 6°45′ N latitude (Fig 1). In both basement areas, the dominant outcropping rocks are crystalline rocks, ranging from phyllites and amphibolites to charnockite and other igneous intrusives (Ekwueme, 2019). Important parts are the Obudu Plateau (part of the Sangwala or Sankwala Mountains) and the Oban Hills. The Oban Massif projects southwards into the Calabar Flank and Mamfe Embayment and eastwards to the Cameroon border (Ekwueme, 2019).

2.2 Local Geology of the Study Area

2.2.1. Geology of the Oban Massif

The resulting geologic map of the Oban Massif, showing lithology and structural trends, is shown in Fig. 1. The Oban Massif is part of the southeastern Nigerian Basement Complex and comprises mainly Precambrian to early Palaeozoic crystalline rocks (Ekwueme & Kröner, 2006; Ekwueme, 2019). The lithologic assemblage includes migmatitic and granitic gneisses, schists, amphibolites, charnockites and pegmatites. Many of these rocks are auriferous. These rocks are intruded by late-stage granites, quartz veins and pegmatitic dykes (Ekwueme, 2019). Structurally, the massif is characterized by NW-SE-trending foliations and ductile shear zones, commonly associated with mineralization. These features are believed to record Pan-African tectonothermal events (ca. 600 Ma) that reworked the older basement lithologies (Ekwueme, 2003).

Shear zones, especially along faulted contacts between gneisses and schists, are favourable conduits for hydrothermal fluids that culminated in gold mineralization (Okonkwo & Folorunso, 2019). On the eastern flank of

the massif, milky and often fractured quartz veins cut both gneisses and schists. These veins, along with sulphide minerals such as pyrite and arsenopyrite, are considered the main hosts of gold mineralization (Ene *et al*., 2021). Alteration halos are common around these mineralized zones and are typically marked by sericitization, silicification and chloritization.

2.2.2 Geology of Obudu Plateau

The Obudu Plateau, located northeast of the Oban Massif, is underlain by Precambrian crystalline basement rocks that form part of the western extension of the Adamawa-Yadé Massif (Ekwueme, 1995; Toteu *et al.,* 2004). The geologic map of the Obudu Plateau, derived from this study and showing lithology and structural trends of the study area, is shown in Fig. 2. The lithology is dominated by medium- to coarse-grained granitic gneisses, migmatites, quartzites, schists, and amphibolites. The plateau is intruded by late-stage pegmatites and quartz veins, some of which are associated with gold occurrences (Okonkwo *et al.,* 2016).

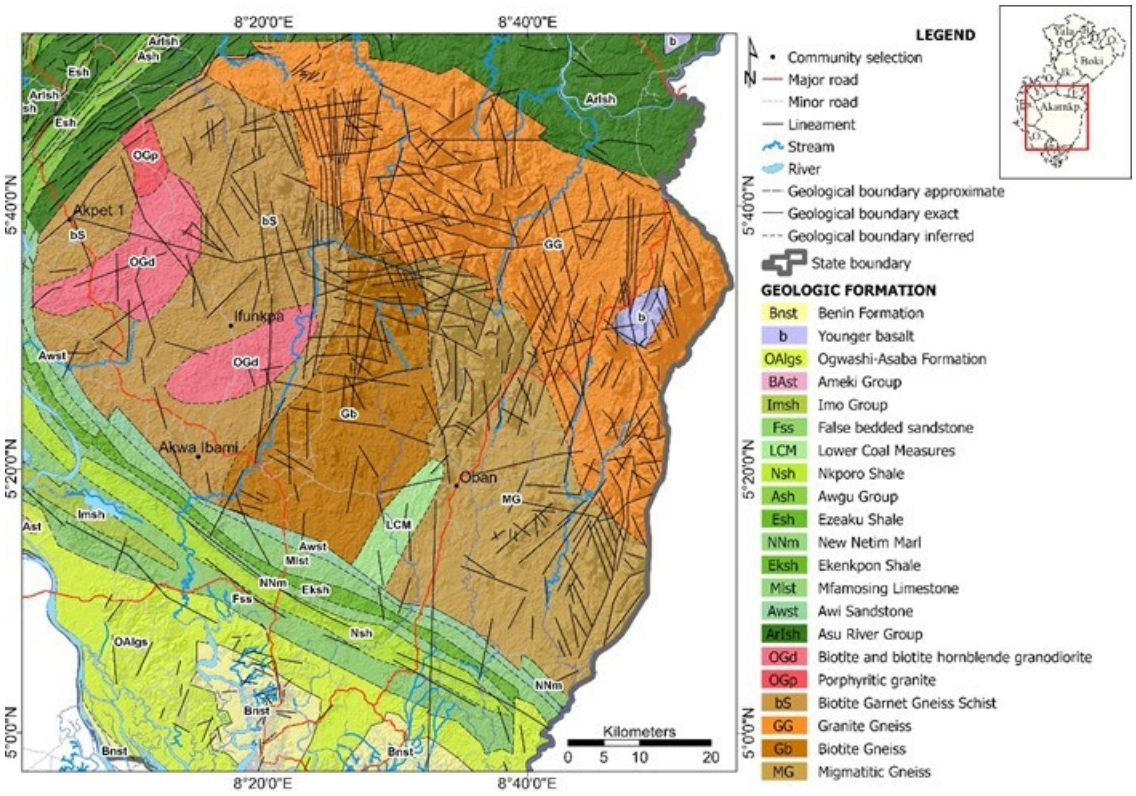

Fig.. 1: Geologic map of the Oban area showing the different structures and drainage pattern

The structural fabric is predominantly NE–SW- and E–W-trending, reflecting multiple deformational episodes. These structures include foliation planes, folds, faults, and ductile shear zones that influence the emplacement of mineralized quartz veins. The tectonic setting indicates that the Obudu Plateau underwent Pan-African reworking similar to that of the Oban Massif, with evidence of high-grade metamorphism reaching amphibolite facies (Ekwueme, 2003; Haruna, 2017).

Hydrothermally formed quartz veins on the plateau are typically hosted within shear zones and contain mineral assemblages of quartz, sericite, chlorite, pyrite, and minor galena. These veins are structurally

controlled, indicating that mineralization is linked to brittle-ductile deformation events that facilitated the circulation of mineralizing fluids during the late stages of tectonism (Toteu *et al*., 2004).

3.0 Materials and Methods

3.1 Field Methods

Field investigations were conducted to confirm geophysical interpretations and to collect representative samples for laboratory analysis. Geological mapping was carried out to identify lithological units, structural features (faults, fractures, folds) and signs of mineralization, such as quartz veins, alteration zones and sulphide occurrences.

Sampling was conducted systematically within the identified target zones. Rock samples were collected from outcrops, veins, and altered zones. Soil samples were collected at depths of 0.5–1.0 m to minimize surface contamination. Stream sediments were collected from active channels to represent upstream geochemical signatures. Sampling points were recorded using GPS. Samples were labelled and stored according to standard protocols to prevent contamination.

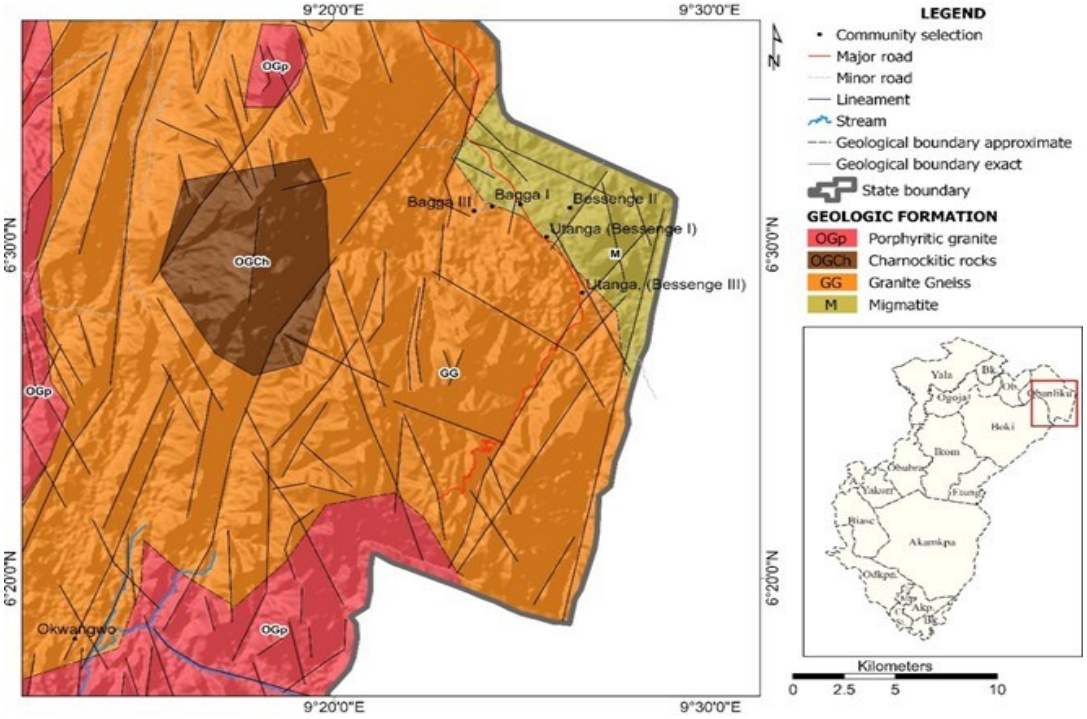

Fig. 2: Geologic map of Obudu area showing the different structures and drainage pattern.

3.2 Laboratory Techniques

3.2.1 Inductively Coupled Plasma Mass Spectrometry (ICP-MS) Analysis

Trace and ultra-trace elemental concentrations, including Au and associated pathfinder elements (As, Pb, Zn, Cu, etc.), were determined by ICP–MS, due to its high sensitivity and multi-element capability.

The samples were dried and homogenized. They were then ground (<75 µm), oven-dried at ~40°C to remove moisture, and homogenized to ensure representativeness, following the procedure detailed by Rollinson (1993). Each sample (0.2-0.5 g) was weighed precisely into Teflon digestion vessels. The samples were digested by a mixed acid system ($HF–HNO_3–HClO_4$) to ensure the complete dissolution of the silicate matrix. Digestion was performed on a hotplate or in a microwave digestion system under controlled temperature conditions (Jarvis & Jarvis, 1992). The digested solution was evaporated to near dryness and re-dissolved in dilute nitric acid (HNO_3) to stabilize it for analysis. Calibration standards were prepared from

certified reference materials (CRMs) across the desired concentration range. Internal standards (e.g., Rh, In) were added to correct for instrumental drift and matrix effects. The liquid sample was nebulized into an aerosol and introduced into the argon plasma (~6000–10,000 K), where it was atomized and ionized. Ions were separated by mass-to-charge ratio (m/z) using a quadrupole mass analyzer and detected with an electron multiplier. Blanks, duplicates and CRMs were used to ensure the accuracy and precision of the analysis. Detection limits and relative standard deviations were verified during the analysis.

3.2.2 Scanning Electron Microscopy–Energy Dispersive Spectroscopy (SEM-EDS)

Mineral morphology and elemental composition at micro- and nano–scales were characterized by SEM–EDS. Rock samples were finely powdered or polished, then mounted on aluminum stubs using conductive carbon tape. A thin layer of gold or carbon was deposited on non-conductive samples to prevent charging under the electron beam, as described by Goldstein (2003). Samples were inserted into the SEM chamber, and a high vacuum was established to transmit the electron beam.

A focused electron beam was incident on the sample surface, generating secondary electrons (SE), backscattered electrons (BSE) and characteristic X-rays. Secondary electron imaging (SE) was used to characterize surface morphology, and backscattered electron imaging (BSE) was used for compositional contrast. The characteristic X-rays emitted from the sample were detected and analyzed for elemental composition, and spectral interpretation was then performed. Spectral interpretation was performed to identify and quantify peaks in the EDS spectrum using software databases. Calibration with known standards was performed to allow accurate identification of the elements. Mineral phase identification and crystallographic analysis were performed using XRD. Sample preparation was the first step in XRD. The samples were ground to a fine powder (<75 μm) and packed into sample holders to ensure a flat, smooth surface. The samples were scanned with a fixed step size and counting time over a 2θ range (typically 5°–70°). The interaction of X-rays with the crystal lattice produced diffraction patterns according to Bragg's Law: $n\lambda = 2d \sin \theta$ (Cullity & Stock, 2001).

Mineral phases were identified by comparing diffraction peaks with standard reference patterns (e.g. ICDD database). Quantitative analysis was performed using relative peak intensities to estimate mineral proportions where needed.

4.0 Results and Discussion

4.1 Results

4.1.1 Major Element Geochemistry of Stream Sediments

Table 1 summarizes the statistical results for major elements (wt.%) from ICP-MS analyses of the Obudu Plateau (Vandikia and Besenge areas) and the Oban Massif (Oban, Okarara, Camp 1 and Camp 4). The variation in element concentrations is shown in the bar charts in the Supplementary Material (S1). The results indicate that the major-element composition of stream sediments from the Obudu–Oban Massif is dominated by silica (Si), with concentrations ranging from 45.10 to 77.61 wt.% (mean = 58.54 wt.%). This suggests a strongly felsic to quartz-rich provenance, consistent with granitic and gneissic basement lithologies.

Aluminium (Al) is moderately enriched (1.01–10.91 wt.%, mean = 4.79 wt.%), consistent with the presence of aluminosilicate minerals such as feldspars and clays. Iron (Fe) is highly variable (1.15-21.47 wt.%, mean = 5.34 wt.%), indicating local enrichment of ferromagnesian minerals and a possible lateritic influence.

Calcium (Ca) and magnesium (Mg) concentrations are highly variable (Ca mean = 0.71 wt.%; Mg mean = 5.45 wt.%), with high Mg values (up to 25.93 wt.% in BSE 1) suggesting input from mafic or ultramafic

components or secondary enrichment processes.

K (0.11–2.84 wt.%) suggests variable feldspar weathering and possible hydrothermal alteration. Titanium (Ti) shows anomalously high values in some samples (up to 15.75 wt.%), indicating heavy-mineral concentration (e.g., ilmenite and rutile).

Sodium (Na) is typically depleted (average = 1.15 wt.%), indicating intense weathering and feldspar breakdown, whereas phosphorus (P) and sulphur (S) occur in trace amounts, suggesting minor inputs from accessory minerals. Overall, the major-element distribution points to a predominantly siliciclastic, felsic source, intense chemical weathering, and localised zones of heavy-mineral enrichment.

Table 1 presents the statistical results for major elements (wt.%) from ICP-MS analyses of the Obudu Plateau (Vandikia and Besenge areas) and the Oban Massif (Oban, Okarara, Camp 1 and Camp 4). The variation in element concentrations is illustrated in the bar charts in the Supplementary Material (S1). The results show that the major-element composition of stream sediments from the Obudu–Oban Massif is dominated by silica (Si), with concentrations ranging from 45.10 to 77.61 wt.% (mean = 58.54 wt.%). This indicates a felsic to quartz-rich provenance, consistent with granitic and gneissic basement lithologies. Aluminium (Al) is moderately enriched (1.01-10.91 wt.%, mean = 4.79 wt.%), reflecting an abundance of aluminosilicate minerals, including feldspars and clays. Iron (Fe) shows a wide range (1.15–21.47 wt.%, mean = 5.34 wt.%), indicating local enrichment of ferromagnesian minerals and a possible lateritic input.

Calcium (Ca) and magnesium (Mg) show highly variable concentrations (Ca mean = 0.71 wt.%; Mg mean = 5.45 wt.%), with high Mg values (up to 25.93 wt.% in BSE 1), suggesting input from mafic or ultramafic components or secondary enrichment processes.

Potassium (K) ranges from 0.11–2.84 wt.%, indicating varying degrees of feldspar weathering and possible hydrothermal alteration. In some samples, titanium (Ti) shows anomalously high values (up to 15.75 wt.%), which may indicate heavy-mineral concentration (e.g., ilmenite, rutile). Sodium (Na) is generally depleted (mean = 1.15 wt.%), reflecting intense weathering and feldspar breakdown. Phosphorus (P) and sulphur (S) are present in trace amounts, reflecting minor contributions from accessory minerals.

Table 1. Summary statistics of major element concentrations (wt.%)

Sample	Fe	Al	Ca	K	Ti	Si	Mn	P	S	Na	Mg
VAN1	2.16	6.73	0.82	2.21	0.10	52.01	0.06	0.0001	0.06	0.001	0.011
VAN2	21.47	3.07	0.07	0.12	15.75	51.93	0.70	0.20	0.002	0.444	0.001
BSE1	3.26	9.77	2.18	1.57	0.39	47.05	0.04	0.07	0.02	3.169	25.93
BSE2	2.28	1.82	0.09	0.83	0.28	65.86	0.02	0.001	0.03	0.001	0.001
UTK	2.59	8.82	2.46	0.11	0.001	53.94	0.03	0.05	0.04	2.952	10.28
BSE3	3.62	2.10	0.21	0.74	1.34	77.61	0.01	0.001	0.01	0.281	0.001
BSE4	3.73	2.19	0.13	1.43	3.11	72.00	0.12	0.001	0.0001	0.004	0.001
OB1	2.09	9.73	0.71	2.84	0.18	45.10	0.03	0.001	0.05	2.164	15.01
OB2	5.52	1.94	0.08	0.28	4.51	71.28	0.22	0.001	0.03	0.001	0.001
OB3	1.15	2.21	0.12	0.56	0.11	65.92	0.01	0.02	0.05	0.001	0.001
OB4	5.02	10.91	2.60	2.13	0.43	59.76	0.06	0.02	0.02	7.004	24.44
OKR	1.25	3.83	0.23	0.43	0.22	58.15	0.02	0.0002	0.01	0.003	0.292
CMP1	18.48	1.01	0.01	0.12	0.27	45.10	0.02	0.001	0.06	0.004	0.016
CMP4	2.18	2.90	0.18	0.45	0.27	53.85	0.02	0.01	0.06	0.074	0.345
Mean	5.34	4.79	0.71	0.99	1.93	58.54	0.10	0.03	0.03	1.15	5.45
SD	6.35	3.57	0.96	0.89	4.19	10.52	0.18	0.05	0.02	2.04	9.55

Table 2. Precious/platinum-group and transition metal concentrations (ppm)

Sample	Au	Pd	Pt	Ir	Os	Ru	Rh	Re	V	Cr	Co	Cu	Zn	Ni
VAN1	0.002	0.497	0.008	0.001	0.001	0.011	0.063	0.047	0.001	0.063	0.001	0.011	46	30
VAN2	0.003	0.124	0.039	0.011	0.002	0.001	0.001	0.016	2.743	0.001	0.001	0.001	122	156
BSE1	0.320	0.187	0.004	0.001	0.063	0.004	0.016	0.063	3.276	0.032	0.014	0.004	64	27
BSE2	0.220	0.311	0.001	0.004	0.001	0.001	0.016	0.001	2.372	0.001	0.002	0.001	11	14
UTK	0.004	0.249	0.001	0.001	0.032	0.001	0.032	0.016	1.616	0.001	0.002	0.023	44	20
BSE3	0.560	2.177	0.003	0.023	0.001	0.083	0.013	0.016	1.698	0.023	0.003	0.001	13	37
BSE4	0.430	3.172	0.001	0.001	0.001	0.001	0.001	0.032	2.090	0.001	0.002	0.016	0	58
OB1	0.550	0.187	0.003	0.001	0.003	0.083	0.003	0.001	1.268	0.016	0.010	0.016	53	33
OB2	0.340	0.498	0.004	0.001	0.001	0.063	0.001	0.002	0.660	0.016	0.001	0.001	29	34
OB3	0.260	0.124	0.005	0.009	0.005	0.001	0.003	0.008	1.156	0.032	0.001	0.001	9	18
OB4	0.330	1.990	0.006	0.006	0.006	0.016	0.028	0.004	2.283	0.001	0.048	0.083	29	35
OKR	0.021	0.001	0.001	0.011	0.001	0.016	0.041	0.021	0.001	0.016	0.001	0.001	28	20
CMP1	0.001	0.002	0.039	0.011	0.021	0.001	0.003	0.016	0.003	0.016	0.002	0.002	17	24
CMP4	0.001	0.124	0.001	0.001	0.001	0.165	0.014	0.003	0.682	0.001	0.002	0.002	22	33
Mean	0.22	0.69	0.01	0.01	0.01	0.03	0.02	0.02	1.42	0.02	0.01	0.01	34.79	38.50
SD	0.20	0.96	0.01	0.01	0.02	0.05	0.02	0.02	1.02	0.02	0.01	0.02	29.89	34.23

Table 3. Selected trace elements (ppm)

Sample	Rb	Sr	Zr	Ba	Nb	Y	Sn	As	Se	Cd	Sb	Pb
VAN1	93	236	0.05	0.29	9	44	48	0.032	1.739	0.032	0.001	0.002
VAN2	0	6	0.90	0.0002	104	107	94	0.001	0.032	0.001	0.002	0.320
BSE1	65	522	0.02	0.07	11	11	0.23	0.001	0.001	0.002	0.002	0.112
BSE2	19	61	0.16	0.04	11	58	21	0.001	0.145	0.003	0.001	0.230
UTK	43	617	0.05	0.12	5	12	33	0.004	0.001	0.007	0.001	0.110
BSE3	12	50	0.43	0.03	15	295	0.23	0.001	0.073	0.001	0.011	0.340
BSE4	0	0	1.05	0.005	78	388	0.0002	0.025	0.001	0.001	0.003	0.330
OB1	203	213	0.07	0.13	13	36	0.001	0.025	0.145	0.016	0.121	23.00
OB2	13	6	0.11	0.001	14	116	0.022	0.001	0.0001	0.016	0.003	0.110
OB3	18	35	0.022	0.03	0	26	0.003	0.016	0.073	0.032	0.001	0.130
OB4	94	291	0.023	0.08	5	54	0.001	0.016	0.217	0.001	0.005	13.00
OKR	15	104	0.16	0.06	0	16	0.002	0.032	0.073	0.003	0.001	2.22
CMP1	14	16	0.03	0.001	0	25	49	0.016	1.087	0.002	0.003	17.00
CMP4	27	37	0.03	0.04	6	28	25	0.016	0.217	0.063	0.002	3.22

Mean	44.00	156.71	0.22	0.06	19.36	86.86	19.32	0.01	0.27	0.01	0.01	4.29
SD	55.34	199.05	0.34	0.08	31.20	114.01	28.38	0.01	0.51	0.02	0.03	7.57

Table 4. Rare earth element concentrations (ppm)

Sample	Pm	La	Ce	Pr	Nd	Sm	Eu	Gd	Tb	Dy	Ho	Er	Y
VAN1	ND	0.221	0.032	0.023	0.001	0.001	0.001	0.001	0.001	0.039	0.001	0.001	44
VAN2	ND	0.042	0.001	0.001	0.028	0.039	0.001	0.003	0.016	0.004	0.016	0.002	107
BSE1	0.016	0.001	0.003	0.016	0.001	0.003	0.016	0.007	0.001	0.001	0.016	0.001	11
BSE2	ND	0.021	0.036	0.001	0.001	0.001	0.016	0.025	0.001	0.001	0.002	0.001	58
...	...	...	...	...	...	...	...	...	...	...	...	...	...
Mean	0.02	0.05	0.06	0.02	0.02	0.01	0.00	0.01	0.06	0.01	0.01	0.01	86.86
SD	0.00	0.07	0.14	0.02	0.03	0.02	0.01	0.01	0.12	0.02	0.01	0.01	114.01

Abbreviations: VAN = Vandikia; BSE = Besenge; UTK = Otukwang; OB = Oban; OKR = Okarara; CMP = Camp. ND = Not Detected. LREE = Light Rare Earth Elements (La–Sm); HREE = Heavy Rare Earth Elements (Eu–Er).

Table 5: Geochemical data and discriminant ratios for samples from the Obudu Plateau and the Oban Massif

Locality	Terrain	Y (ppm)	Rb (ppm)	Nb (ppm)	Sr (ppm)	La (ppm)	Y + Nb	Rb/Sr	Rb/Y	Rb/ (Y+Nb)	Nb/Y
Vandikia 1	Obudu	44	93	9	236	0.221	53	0.39	2.11	1.75	0.20
Vandikia 2	Obudu	107	0	104	6	0.042	211	0.00	0.00	0.00	0.97
Besenge 1	Obudu	11	65	11	522	0.0012	22	0.12	5.91	2.95	1.00
Besenge 2	Obudu	58	19	11	61	0.021	69	0.31	0.33	0.28	0.19
Otukwang	Obudu	12	43	5	617	0.0321	17	0.07	3.58	2.53	0.42
Besenge 3	Obudu	295	12	15	50	0.191	310	0.24	0.04	0.04	0.05
Besenge 4	Obudu	388	0.021	78	0.0012	0.085	466	0.18	0.00	0.00	0.20
Oban 1	Oban	36	203	13	213	0.0013	49	0.95	5.64	4.14	0.36
Oban 2	Oban	116	13	14	6	0.021	130	2.17	0.11	0.10	0.12
Oban 3	Oban	26	18.03	0	35	0.0011	26	0.52	0.69	0.69	0.00
Oban 4	Oban	54	94	5	291	0.0015	59	0.32	1.74	1.59	0.09
Okarara	Oban	16	15	0	104	0.021	16	0.14	0.94	0.94	0.00
Camp 1	Oban	25	14	0	16	0.0012	25	0.88	0.56	0.56	0.00
Camp 4	Oban	28	27	6	37	0.013	34	0.73	0.96	0.79	0.21

The major-element distribution generally indicates a predominantly siliciclastic and felsic source, strong chemical weathering, and localized areas of heavy-mineral enrichment.

4.1.3 Tectonic Setting and Evolution

Table 5 presents compiled geochemical data and calculated discriminant ratios used in tectonic discrimination diagrams for stream sediment samples from the Obudu Plateau and the Oban Massif. Fig. 3. Trace element discrimination diagrams of (a) Rb vs. Y+Nb, (b) Rb/(Y+Nb), and (c) Nb vs. Rb.

The Rb vs. (Y+nb) discrimination diagram of Pearce *et al*. (1984) is one of the most widely used geotectonic tools for granitic rocks. The diagram divides granite suites into four main tectonic fields: volcanic arc granites (VAG), within-plate granites (WPG), syn-collisional granites (syn-COLG), and ocean ridge granites (ORG). In the present study, samples from basement terrains show contrasting yet overlapping distributions.

Samples from the Obudu Plateau (localities Vandikia, Besenge, Otukwang) show a bimodal scatter across the VAG-syn-COLG boundary and into the WPG field. Three samples (Besenge 3; Besenge 4, and Vandikia 2) show exceptionally high Y+Nb values (310–466 ppm) and plot well within the WPG field at relatively low Rb concentrations (Rb 15 ppm for Besenge 3 and Besenge 4). The anomalously low Rb in Besenge 4 (Rb ~0.0002 ppm) is noteworthy and may indicate significant post-magmatic depletion or extreme alteration/leaching. By contrast, the Vandikia 1, Besenge 1, and Otukwang samples fall within the syn-COLG–VAG boundary field (Y+Nb = 17–53 ppm; Rb = 43–93 ppm), typical of a compressional arc-collisional setting.

The samples from the Oban Massif (Oban 1–4, Okarara, Camp 1; Camp 4) mostly fall within the syn-COLG to VAG fields and are moderately enriched in Y+Nb (16–130 ppm) and Rb (13–203 ppm). Oban 1 lies within the syn-COLG field (Y+Nb = 49 ppm; Rb = 203 ppm), whereas Oban 2 plots at the WPG–VAG boundary with a moderate Y+Nb of 130 ppm. Camp samples and Okarara show low Y+Nb (16–34 ppm) and variable Rb (14–27 ppm), suggesting arc-related settings. Overall, the Oban dataset is representative of dominantly convergent-margin magmatism with some within-plate overprinting.

The modified Pearce (1996) diagram normalises Rb to (Y + Nb), improves discrimination between syn-collisional and volcanic-arc environments, and separates ORG from the other fields. The Obudu Plateau samples are more dispersed on this diagram. Besenge 1 and Otukwang produce high Rb/(Y+Nb) values (2.95 and 2.53, respectively) that plot in the syn-COLG to upper VAG field. Vandikia 1 (Rb/(Y+Nb) = 1.75; Y+Nb = 53 ppm) also falls in the syn-COLG field. The Y-rich samples (Besenge 3; Besenge 4, Vandikia 2) show very low Rb/(Y+Nb) ratios (< 0.1), typical of ORG-type or highly fractionated within-plate affinity.

Oban 1 has the highest Rb/(Y+Nb) ratio (4.14) in the Oban Massif, clearly within the syn-COLG field. The Rb/(Y+Nb) ratios of Oban 3, Oban 4 and the Camp localities range from 0.56 to 1.59, spanning the VAG-syn-COLG boundary. Oban 2 (Rb/(Y+Nb) = 0.10; Y+Nb = 130 ppm) plots near the WPG–VAG boundary, consistent with a mixed or transitional tectonic affinity. The Oban Massif was interpreted as predominantly formed in a convergent tectonic setting, with minor extensional or intraplate effects.

The Schandl and Gorton (2002) Nb/Y vs. Rb/Sr discrimination diagram separates active continental margins (ACM), within-plate continental settings (WP), continental margin arcs (CMA), and MORB/ORG settings. It is highly sensitive to crustal contamination and to subduction-related depletion of high-field-strength elements (HFSEs).

Obudu Plateau samples are distributed across three distinct zones. Vandikia 2 and Besenge 1 plot within the within-plate (OIB-like) field, with high Nb/Y ratios (~0.97–1.00) and low-to-moderate Rb/Sr ratios. Besenge 3, Besenge 4 and Besenge 2 plot near the MORB–ORG boundary, with low Nb/Y (0.05–0.20) and variable Rb/Sr. Otukwang and Vandikia 1 plot in the continental margin arc (CMA) to VAG zone, characterised by Nb/Y between 0.2 and 0.42 and Rb/Sr between 0.07 and 0.39. The diversity of rock types suggests that the Obudu Plateau experienced multi-stage magmatic events in both intraplate and arc settings during the Pan-African orogeny.

Samples from the Oban Massif are primarily from the ACM and WP fields. Oban 1 (Rb/Sr = 0.953; Nb/Y = 0.361) lies on the CMA–ACM boundary, whereas Oban 2 (Rb/Sr = 2.17; Nb/Y = 0.121) plots clearly within the active continental margin (ACM) field, suggesting a subduction-modified source. Camp 1 (Rb/Sr = 0.875; Nb/Y = 0.000) and Oban 3 (Rb/Sr = 0.515; Nb/Y = 0.000) fall within the ACM field and contain no detectable Nb, consistent with strongly arc-influenced melts. Oban 4 and Camp 4 straddle the CMA–WP transition, indicating mixed source characteristics typical of post-collisional magmas intruded during crustal relaxation.

The Obudu Plateau samples cover a wider tectonic spectrum of within-plate, syn-collisional and arc settings, whereas the Oban Massif samples are more tightly constrained to arc-collisional (VAG/syn-COLG/ACM) settings. Both terrains contain samples with anomalous geochemical signatures that require explanation in terms of petrogenetic processes beyond simple end-member tectonic models (Table 6).

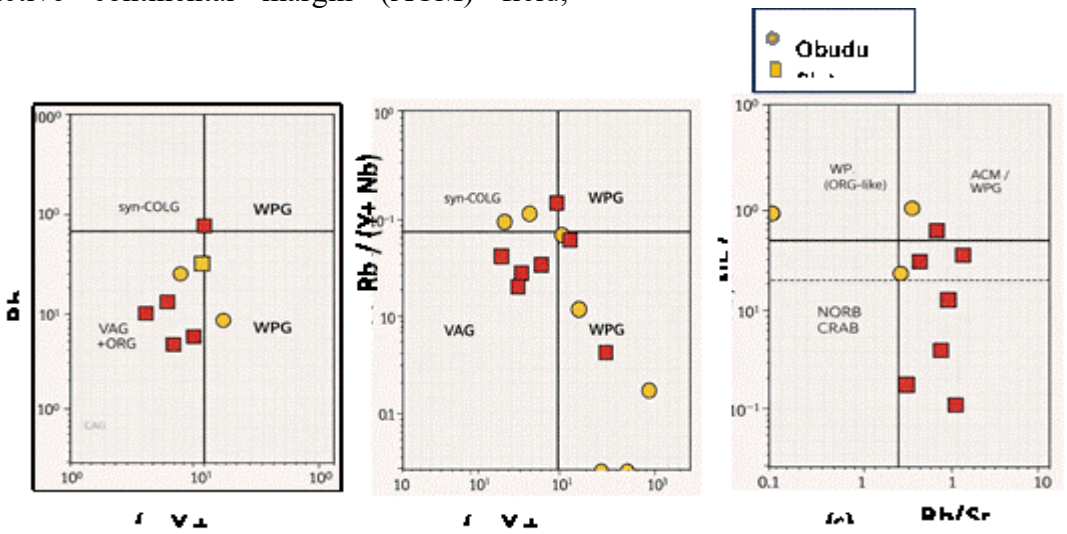

Fig. 3: Trace element discrimination diagrams of (a) Rb vs Y+Nb (Pearce *et al*., 1984), (b) Rb/(Y+Nb) vs Y+Nb (Pearce, 1996), and (c) Nb/Y vs Rb/Sr (Schandl & Gorton, 2002)

4.1.4 Shape and Internal Configuration of Gold Grains

Free gold grains were recovered by panning from two stream localities within the Obudu-Oban Massif: Besenge 3 stream (Obudu Plateau) and Oban 1 stream (Oban Massif). After panning, the grains were mounted in epoxy resin, polished, carbon-coated, and analyzed using Backscattered Electron (BSE) imaging combined with Energy-Dispersive Spectroscopy (EDS) and Electron Probe Micro-Analysis (EMPA). Fig. 4 shows BSE images and representative EDS spectra. Tables 7-8 present EMPA data on mineral inclusions and gold alloy microchemistry.

4.1.4.1 Morphology and Microtextural Features of Gold Grains

BSE imaging shows that gold grains from both localities are predominantly subrounded in outline. The Oban 1 grains are moderately

smoothed, consistent with moderate fluvial transport and abrasion. The Besenge 3 grains are also subrounded but locally retain angular microdomains with pitted surface textures. Polished cross-sections of both grain sets show a distinct core-rim microtexture: darker cores are surrounded by BSE-brighter (higher mean atomic number) outer zones, consistent with Ag depletion in the rim relative to the Au-Ag alloy core. This zonation is well developed in Grain 3 from Oban 1, with the core containing 6.33 wt% Ag and the rim 2.45 wt% Ag. No secondary authigenic gold precipitates (e.g., bacterioform gold or microspherulites) were found on grain surfaces, confirming that the grains' primary detrital character is preserved.

Mineral inclusions detected by EDS in the gold grains differ markedly between the two localities. The Oban 1 grain has one sub-rounded inclusion of cassiterite (SnO_2). The Besenge 3 grains contain two euhedral monazite inclusions characterized by a Ce-La-Nd-P-dominated composition. The contrasting inclusion assemblages, a resistate oxide mineral (cassiterite) at Oban 1 versus euhedral phosphate mineral (monazite) at Besenge 3, suggest fundamentally different primary gold-forming environments in the two massif domains.

Table 6: Summary of the integrated results of the three discrimination diagrams

Locality	Terrain	Rb vs Y+Nb	Rb/(Y+Nb) vs Y+Nb	Nb/Y vs Rb/Sr
Vandikia 1	Obudu	syn-COLG / VAG	syn-COLG	CMA
Vandikia 2	Obudu	WPG	ORG / WPG	WP (OIB-like)
Besenge 1	Obudu	syn-COLG	syn-COLG	WP (OIB-like)
Besenge 2	Obudu	VAG	VAG	MORB / ORG
Otukwang	Obudu	syn-COLG / VAG	syn-COLG	CMA
Besenge 3	Obudu	WPG	ORG	MORB
Besenge 4	Obudu	WPG	ORG	MORB / ORG
Oban 1	Oban	syn-COLG	syn-COLG	CMA / ACM
Oban 2	Oban	WPG / VAG	WPG / VAG	ACM
Oban 3	Oban	syn-COLG / VAG	VAG	ACM
Oban 4	Oban	syn-COLG / VAG	VAG / syn-COLG	CMA / WP
Okarara	Oban	VAG / ORG	VAG	ACM
Camp 1	Oban	VAG / ORG	VAG	ACM
Camp 4	Oban	VAG	VAG	CMA / WP

4.1.4.2 Gold microchemistry

Gold fineness is expressed as F = Au/ (Au + Ag) × 1000, where F is the fineness in parts per thousand. EMPA alloy data for both localities are given in Tables 8a-b. All analytical totals are close to 100 wt.%, indicating reliable data.

Gold concentrations range from 92.87 to 100.00 wt.% Au, Ag from 0.00 to 6.33 wt.%, and Cu from 0.00 to 1.16 wt.%. One analysis report 2.84 wt.% N (analytical artefact). Fineness values range from 936.19 to 1000.00. The three core analyses (spots B, C, D on a single grain) return F = 1000.00 and no detectable Ag. These are very pure gold cores. Fig. 3 shows a decrease in Ag content from core to rim. The core (spot A) has an Au content of 92.87 wt.%. Ag = 6.33 wt.% (F = 936.19), and the corresponding rim (spot B) has Au = 96.39 wt.%, Ag = 2.45 wt.% (F = 975.21), showing a clear supergene Ag-depletion gradient from core to rim. Minor Cu (≤1.16 wt.%) occurs in both the core and rim analyses. Gold concentrations in Oban 1

stream are consistently high (96.55-98.90 wt.% Au), with low Ag (0.43-2.48 wt.%) and minor Cu (0.41-0.98 wt.%). Totals for all analyses are ~99.99-100.01 wt.%. Fineness values are consistently high and tightly clustered between 989.95 and 995.87 (mean ~992.9), indicative of a homogeneous, nearly pure gold alloy. Rim spots contain slightly lower Ag than core spots within the same grain, exhibiting a weak but consistent pattern of Ag depletion, similar to that seen at Oban 1 but much less pronounced.

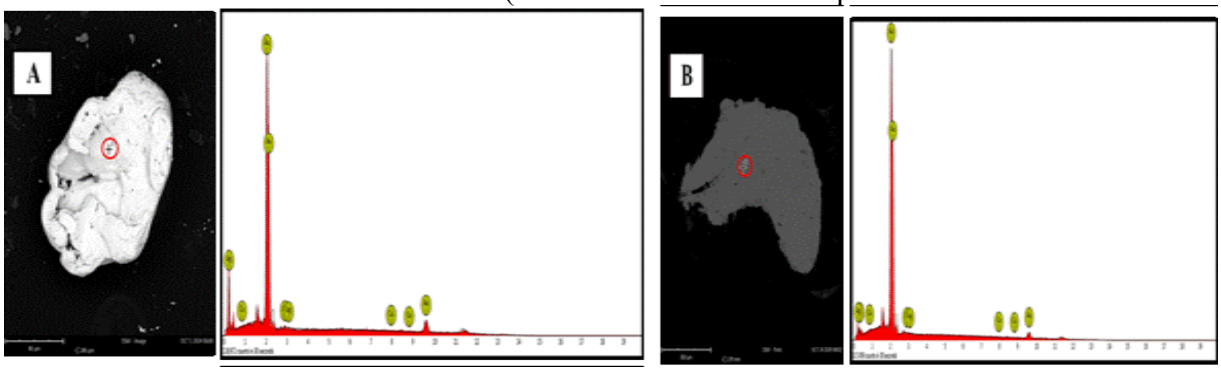

Fig. 4: BSE images and EDS spectra of gold grains from (A) Oban 1 stream and (B) Bessenge 3. The red circles represent the analytical spots

Table 7a: EMPA data of gold inclusions from the Oban massif

Parameter	Inclusion 1
Location	Oban Stream
O	46.78
Si	–
Al	–
K	–
Sn	53.22
C	–
Fe	–
Ca	–
Mg	–
Total	100.00
Mineral Inclusion	Cassiterite
Shape of Inclusion	Sub-rounded

Table 7b: EMPA data of gold inclusions from the Obudu Plateau

Parameter	Inclusion 1	Inclusion 2
Location	Besenge	Besenge
O	59.48	55.49
Si	–	1.68
Al	–	1.61
K	–	–
Sr	–	–
Ce	11.73	12.55
P	8.78	7.78
Pr	0.53	0.50

Sm	0.31	1.07
Pm	0.00	0.00
Gd	0.00	0.79
Dy	0.00	0.54
La	5.52	6.75
Zr	6.04	5.07
Nd	4.47	–
Nb	–	–
Ho	–	0.00
C	0.82	4.96
Ti	–	–
Ag	2.32	1.22
Fe	–	–
Na	–	–
Ca	–	–
Total	100.00	100.01
Mineral Inclusion	Monazite	Monazite
Shape of Inclusion	Euhedral	Euhedral

Table 8a: EMPA data of gold inclusions from the Oban Massif

Spot	Zone	Au (wt.%)	Ag (wt.%)	Cu (wt.%)	Total (%)	Fineness
B	Core	97.16	0.00	0.00	100.00	1000.00
C	Core	100.00	0.00	0.00	100.00	1000.00
D	Core	98.96	0.00	1.04	100.00	1000.00
A	Core	92.87	6.33	0.80	100.00	936.19
B	Rim	96.39	2.45	1.16	100.00	975.21

**** Grain = 3, N Wt% = 2.84**

Table 8b: EMPA data of gold inclusions from the Obudu plateau

Location/Grain (Bessenge 3 Stream, Grain 3)	Spot	Zone	Au (wt%)	Ag (wt%)	Cu (wt%)	Total (%)	Fineness
B	Core	Core	96.65	2.48	0.87	100.00	991.08
C	Core	Core	97.57	1.91	0.52	100.00	994.70
D	Rim	Rim	98.83	0.43	0.73	99.99	992.67
A	Rim	Rim	96.55	2.46	0.98	99.99	989.95
B	Rim	Rim	98.90	0.70	0.41	100.01	995.87

4.1.4 Statistical analysis

Results of the rotated varimax principal component analysis of major, trace, and REE are shown in S5. Table 9 presents the extracted components, their variance contributions, and the loadings of the dominant elements, while Figs. 4 and 5 show the component plots in the rotated space and the scree plot, respectively. Rotated varimax principal component analysis (PCA) was performed on the standardized ICP-MS geochemical dataset comprising 49 variables (major, trace, and rare-earth elements) from 14 stream-sediment samples collected from the Obudu-Oban Massif. Using eigenvalues greater than 1.0 (Kaiser criterion), eleven statistically significant principal components

(PCs) were extracted, collectively explaining 96.47% of the total variance in the dataset (Table 9). The rotated component matrix (Varimax-normalized) maximizes the variance of the squared loadings of a factor (component) across all variables in the factor matrix, thereby helping identify geochemical element groupings and their controlling processes (Rollinson, 1993).

The scree plot of the eigenvalues shows a clear elbow after the fifth component, indicating that the first five PCs capture the dominant variance structure of the dataset (cumulative 71.05%), whereas PCs 6–11 capture progressively smaller but still geochemically meaningful contributions (cumulative 96.47%). The component plots in rotated space show distinct spatial clustering of element groups, consistent with lithological, weathering-related, and mineralization-associated influences on stream-sediment composition.

Table 9: Summary of Varimax-Rotated Principal Component Analysis (PCA) Showing Variance Contributions and Dominant Element Loadings from ICP–MS Geochemical Data of Stream Sediments in the Obudu–Oban Massif

PC	EV	%σ	C%	Dominant Element Loadings (|r| > 0.50)	Interpretation
PC1	10.84	22.12	22.12	Mn (0.97), Ni (0.97), Ti (0.95), P (0.91), Zn (0.86), Nb (0.81), Sn (0.72), Fe (0.71), Zr (0.58), Pt (0.64)	Mafic/ultramafic heavy mineral placer + Fe-Ti oxide
PC2	7.93	16.18	38.3	Ce (0.97), Y (0.94), Pd (0.92), Nd (0.69), Dy (0.77), Zr (0.75), Si (0.60), Au (0.49)	REE-PGE hydrothermal-pegmatitic + siliceous carrier
PC3	6.88	14.04	52.34	Na (0.97), Co (0.95), Cu (0.93), Ca (0.84), Mg (0.82), Al (0.76), Sr (0.55)	Mafic/calc-silicate provenance + plagioclase weathering
PC4	4.95	10.11	62.45	Cr (0.82), La (0.82), Ba (0.80), Rh (0.74), Se (0.66), Re (0.51)	Chromite-bearing mafic lithology + LREE enrichment
PC5	4.22	8.61	71.05	Sm (0.89), Tb (0.93), Ir (0.68), Pt (0.60), Fe (0.56), Pb (0.39)	MREE-HREE fractionation + sulphide/PGE mineralization
PC6	3.92	7.99	79.05	Sb (0.97), Rb (0.83), K (0.69), Pb (0.69)	Epithermal-hydrothermal / K-feldspar + antimony pathfinder
PC7	2.38	4.85	83.9	As (0.72), V (-0.61), Eu (-0.71), Dy (0.47)	Arsenical pathfinder for Au + negative Eu anomaly
PC8	2.09	4.26	88.16	Ru (0.81), Cd (0.81), Er (0.89), Ho (0.70)	HREE (Er-Ho) + PGE (Ru) placer / heavy mineral
PC9	1.82	3.71	91.87	Os (0.83), Re (0.78), Sr (0.48), Eu (0.39)	Os-Re PGE / mafic intrusion indicator
PC 10	1.24	2.53	94.4	Pr (-0.87)	LREE (Pr) fractionation / monazite or allanite
PC 11	1.01	2.07	96.47	Gd (0.61), Nd (0.50)	MREE Gd-Nd / secondary REE mineral phase

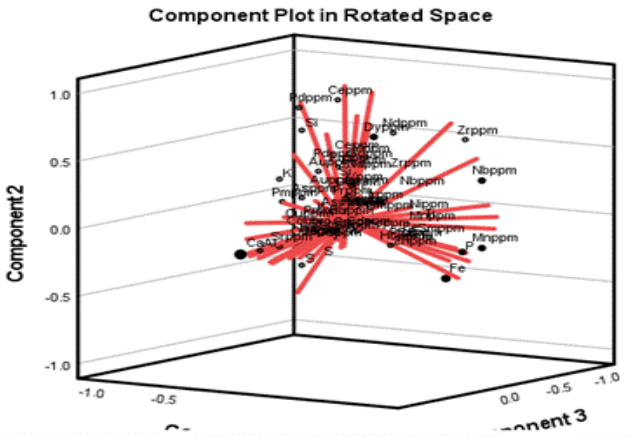

Fig. 4: Component plots in rotated space

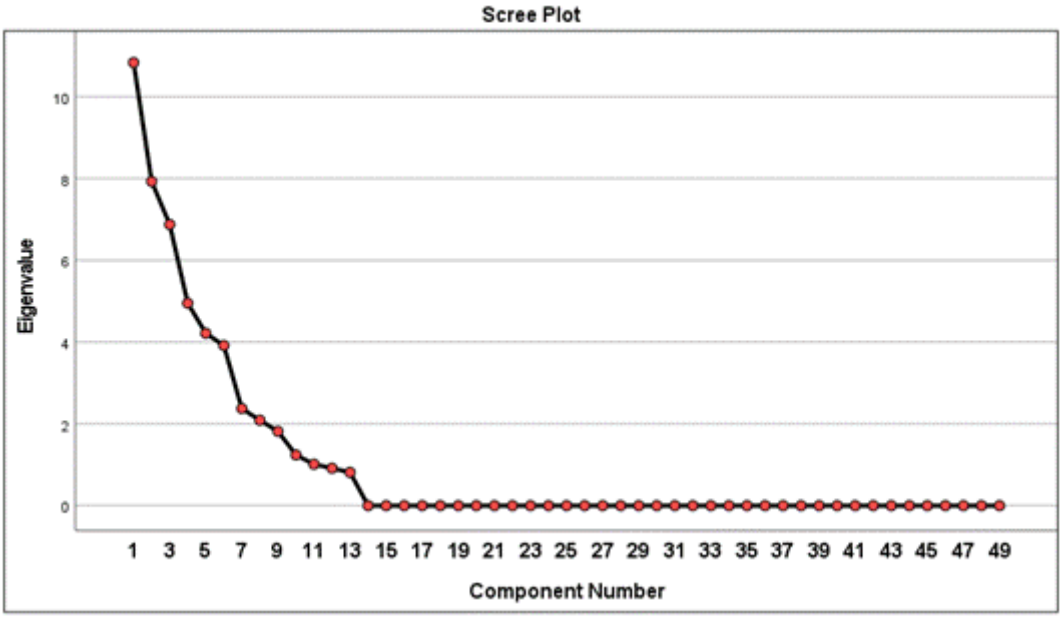

Fig.. 5: Scree plot showing the eigenvalue of the extracted principal components

3.2 Discussion

3.2.2 Implications of major, trace and rare element geochemistry for provenance, weathering processes and mineral exploration

The integrated ICP-MS geochemical dataset for stream sediments from the Obudu–Oban Massif provides important clues to provenance, weathering intensity, and mineralization potential within this Precambrian terrain. The results point to a geochemical system affected by siliciclastic influx, with localized, superimposed hydrothermal and potential magmatic signatures associated with gold and rare-metal mineralization

Trace-element distributions provide additional constraints on the mineralization potential of the study area. Gold (Au) ranges from 0.001 to 0.56 ppm (mean 0.22 ppm), which is considerably higher than the average upper-continental-crust value (~0.004 ppm) and reflects significant geochemical anomalies. The highest Au concentrations in the Besenge 3 and Oban 1 samples suggest the presence of proximal primary mineralization sources. The correlation between Au and pathfinder elements such as As, Sb, and Pb supports a hydrothermal

origin, consistent with orogenic gold systems, which are usually controlled by shear zones and fault structures (Groves *et al*., 1998). Similar gold anomalies have been reported in the schist belts of south-western Nigeria and the Birimian terranes of Ghana, where structurally controlled mineralization is a dominant feature (Hilson, 2002; Olade, 2021).

The platinum group elements (PGEs) are present in low overall concentrations, but palladium (Pd) is locally enriched (up to 3.17 ppm) relative to platinum (Pt). This Pd-dominated signature may be related to fractionation during hydrothermal processes and/or limited input from mafic-ultramafic sources. Elevated Ni (up to 156 ppm) and moderate Zn abundances support minor contributions from mafic lithologies, although generally low Co, Cu, and Cr abundances suggest that primary magmatic sulphide mineralisation is not a dominant process in the study area. Similar geochemical features have been described from Pan-African belts where the distribution of trace metals was controlled by crustal reworking and limited mantle input (Barnes & Lightfoot, 2005).

Large-ion lithophile elements (LILE) and high-field-strength elements (HFSE) show great variability, indicating complex petrogenetic and weathering processes. Rubidium (Rb) and strontium (Sr) distributions indicate varying degrees of feldspar alteration, while high niobium (Nb), yttrium (Y), and tin (Sn) contents in some samples suggest the involvement of evolved granitic or pegmatitic systems. Enrichments of this type are characteristic of rare-metal-bearing granites and have also been frequently reported from the Nigerian Younger Granite Province and other Pan-African terranes (Kinnaird, 1985). The observed HFSE enrichment suggests that parts of the study area may host economically valuable concentrations of rare metals, especially Nb and Sn, which are typically associated with highly fractionated granitic systems.

The distributions of rare earth elements (Table 4) also provide insights into the geochemical evolution of the sediments. The dataset shows a general enrichment of light rare-earth elements (LREEs) over heavy rare-earth elements (HREEs), consistent with derivation from felsic crustal sources (Table x, Appendix x). This fractionation pattern reflects processes such as partial melting, fractional crystallization, and the preferential incorporation of LREEs into accessory minerals such as monazite. The localized enrichment of Y and HREEs in some samples indicates the presence of heavy mineral phases such as zircon and xenotime, which are important sources for these elements. Similar REE patterns have been observed in the granitoid terrains of the Nigerian Basement Complex and other African Precambrian shields (Rollinson, 2014; Omang *et al*.,2023).

Integrated major-, trace-, and REE geochemistry indicates a multi-source sediment system with contributions from felsic basement rocks, minor mafic input, and hydrothermal processes. The geochemical signatures strongly suggest that the mineralization within the Obudu – Oban Massif is structurally controlled and may be related to shear zones and intrusive contacts. This interpretation agrees with aeromagnetic-based structural delineations usually reported in similar geological settings.

Regarding exploration, the results have identified several high-potential targets. The Besenge and Oban areas exhibit strong gold anomalies and associated pathfinder elements, making them priority zones for follow-up exploration, including detailed geophysical surveys and drilling. The enrichment of Nb, Sn and Y suggest the possibility of rare-metal mineralization, particularly in areas affected by granitic intrusions or pegmatitic activity. Furthermore, the presence of REEs and HFSEs suggests the possibility of radiogenic

mineralization of uranium and thorium, which are typically associated with evolved felsic systems.

The geochemical characteristics of the study area are similar to those of mineralized Precambrian terranes, such as the Birimian belts of West Africa and the Pan-African mobile belts of Central Africa (Toteu *et al*., 2004), as well as to other geological settings worldwide. These analogues corroborate the study area's high mineral resource potential, particularly for gold and rare metals. The high Au anomalies, REE enrichment, and HFSE signatures emphasize the importance of integrating geochemical, geophysical, and geological datasets for exploration.

In summary, geochemical data provide strong evidence for a mineralized system in the study area with felsic provenance, severe tropical weathering and hydrothermal enrichment. These results not only confirm the region's exploration potential but also provide a strong geochemical framework to guide future mineral exploration and sustainable resource development in south-eastern Nigeria.

4.2.2 Tectonic Setting and Evolution

The trace-element discrimination diagrams (Fig. 3) show that the geochemical signatures of the Obudu Plateau and the Oban Massif are broadly consistent with magmatism associated with the Pan-African orogeny (~900-550 Ma), which culminated in the amalgamation of the West African, Congo, and São Francisco cratons during the assembly of Gondwana. The dominance of syn-COLG and VAG fields in both terrains (Fig. 3) is consistent with the prevailing model of subduction-driven arc magmatism followed by continent-continent collision as documented in analogous Pan-African basement terrains across West and Central Africa (Nzenti *et al*., 2006).

The syn-COLG affinity of several of the Obudu Plateau and Oban Massif samples can be directly compared with observations by Ferré *et al*. (2002) in the Central African fold belt, where post-collisional granites with high Rb and moderate Y+Nb are interpreted as products of melting of thickened crust following the termination of subduction. Similarly, syn-COLG granites with overlapping geochemical parameters were documented by Toteu *et al*. (2004) in the Yaoundé Belt of northern Cameroon, a geologically contiguous terrain to the Nigerian basement to the west. In particular, the geochemical affinities of the Oban Massif are similar to those of the Adamawa basement of Cameroon, where ACM-dominated tectonic signatures were also reported by Nzenti *et al*. (2006) in high-grade metamorphic and granitoid rocks.

A subset of Obudu Plateau samples (Vandikia 2; Besenge 1; Besenge 3; Besenge 4) plot consistently in WPG or OIB-like fields in all three discrimination diagrams, with anomalously high Y+Nb (211-466 ppm) and high Nb/Y ratios close to unity (Fig. 3). These signatures are not typical of simple crustal melts and imply either partial melting of an asthenospheric or enriched lithospheric mantle source with OIB-like geochemical characteristics, extensional tectonic overprinting after the collisional phase, or contamination by HFSE-enriched lower-crustal material.

Several global Pan-African and Proterozoic basement terrains have reported high-Nb granitic rocks with OIB affinities. Post-collisional A-type granites showing within-plate signatures in the Arabian Nubian Shield (ANS) have been described by Johnson (2011) and are interpreted as products of delamination-triggered asthenospheric upwelling following the Pan-African orogenic belt thickening. High Y and Nb-analogue WPG/A-type rocks have been described from the Nigerian Younger Granites province (Wright, 1985), where magmatism at ~150 Ma is attributed to an intraplate hotspot. A more parsimonious explanation is that these rocks represent late-stage Pan-African extensional or post-collisional magmatism analogous to that described by Tack & Bowden (1999). in the

Hoggar massif of Algeria, where A-type and transitional granites intruded during the post-orogenic collapse of the Trans-Saharan belt, because the WPG-signature Obudu samples are Precambrian basement rocks rather than Jurassic ring complexes.

4.2.2.1 Comparison of the tectonic signatures with other Nigerian Basement Provinces

The Obudu and Oban terrains of the Nigerian basement complex are broadly similar to the Older Granites belt but are geochemically different from the anorogenic Jurassic Younger Granites. Chukwu, & Obiora, (2021) have reported syn-COLG to WPG granites in the Nasarawa area of north-central Nigeria with Rb vs (Y+Nb) distributions similar to those presented here, attributing the magmatic diversity to multi-phase Pan-African tectonism involving both subduction and subsequent crustal extension. The elevated Rb/Sr ratios (> 0.5) in some of the samples from the Oban Massif (Oban 1–4, Camp 1) are consistent with the high Rb/Sr in the granites of the Jos Plateau and Ilesha schist belt, where post-collisional fractionation and crustal melting have been invoked (Dada, *et al*., 2024). The Cameroon Highlands immediately east of Obudu may be the closest geological analogue. Tectonic discrimination plots for basement granites from the Bamenda Highlands, straddling the VAG–syn-COLG boundary and including accessory WPG outliers, were reported by Asaah *et al*. (2015) – a pattern almost identical to the Obudu dataset. This continuity across the Nigeria-Cameroon border favours the interpretation that both the Obudu Plateau and the neighbouring Cameroonian basement are fragments of a single, coherent Pan-African orogenic domain, subsequently rifted and dismembered during the Cretaceous opening of the Benue Trough.

Both Obudu Plateau and Oban Massif are adjacent to the Cretaceous Benue Trough, a failed arm of the South Atlantic rift. Some of the anomalies in the WPG and ACM found in some samples may partly reflect rift-related thermal perturbation and crustal thinning that preceded and accompanied the formation of the Benue Trough (~130–65 Ma). Benkhelil (1982) observed that basement rocks adjacent to the Benue Trough reflect extensional strain and associated hydrothermal alteration, which would be expected to alter trace-element ratios such as Rb/Sr by Sr depletion and Rb enrichment due to potassic metasomatism. The very high Rb/Sr ratio in Oban 2 (2.17) may reflect such a fluid-rock interaction overprint rather than a primary tectonic signal.

4.2.3 Implication of tectonic discrimination to mineralisation potential

The results of the tectonic discrimination are of great importance for the mineral resource potential of both terrains.

The majority of the Obudu and Oban samples are strongly associated with syn-collisional (syn-COLG) and volcanic arc (VAG) settings, which are associated with orogenic gold deposits, W-Sn-Mo mineralisation in greisen and skarn systems, base-metal (Cu-Zn-Pb) volcanogenic massive sulphide (VMS) deposits and Fe-oxide copper-gold (IOCG) systems. The high Rb and moderate Sr contents of syn-COLG samples suggest a high-K granitic source, typical of S-type and I-type collision granites that host scheelite- and cassiterite-bearing pegmatites worldwide. Hence, the syn-COLG granites of the Obudu Plateau (Vandikia, Besenge, Otukwang localities) are potential hosts for W-Sn mineralisation akin to the economically important tin-tungsten deposits of the Hoggar (Algeria) and the Jos Plateau Younger Granites in Nigeria, although the latter are of anorogenic affinity.

Besenge 3 and 4, and Vandikia 2 in particular, are geochemically similar to the A-type granites, which host Nb-Ta-REE-Zr mineralization worldwide. Concentrations of high-field-strength elements (HFSE) in these samples suggest the potential for columbite-tantalite and zircon-bearing pegmatites, as well as carbonatite-related REE

mineralization. In Nigeria, the columbite belt (Jos Plateau) is hosted within comparable peralkaline and A-type granite systems (Whalen *et al*., 1987). The Obudu WPG-affinity samples may therefore represent a southward extension of this mineralized corridor and be the subject of targeted geophysical surveys and pegmatite mapping.

Samples from the Oban Massif (notably Oban 2, Okarara, Camp 1) on an active continental margin (ACM) exhibit high Rb/Sr and little or no Nb, characteristic of subduction-related calc-alkaline magmatism. Porphyry Cu-Mo and epithermal Au-Ag systems are found in such environments worldwide. The Nb-depletion and high Rb/Sr ratios are diagnostic of arc magmas with fluid-saturated source regions, which is precisely the environment favourable for porphyry copper formation, as described in the Andean arc systems (Richards, 2022) and in similar Pan-African arc terrains of the ANS (Harbi *et al*., 2019). Economic porphyry-style deposits have not been formally identified in the Oban Massif, but the geochemical evidence presented here warrants further investigation, particularly around hydrothermal breccia zones and contact aureoles.

The Rb/Sr ratios in both terrains are also instructive of the potential for gold. High Rb/Sr (>0.3) in granites has been empirically linked to orogenic gold endowment (Groves *et al*., 2003) and has been applied to prospectivity assessments in West African terranes (Feybesse *et al*., 2006). Several samples from the Oban Massif (Oban 1: 0.953; Oban 2: 2.167; Camp 1: 0.875; Camp 4: 0.730) and Obudu Plateau (Vandikia 1: 0.394; Besenge 2: 0.311) exceed or approach this threshold, suggesting meaningful gold prospectivity in both terrains.

4.2.4 Implication of Gold Grain Morphology, Microtexture, Placer Maturity and Transport Distance

The sub-rounded morphology of gold grains from both Oban 1 and Besenge 3 provides a first-order constraint on transport distance from the primary lode source. Based on the widely used classification of gold grain morphologies, angular to sub-angular grains with pristine crystal faces are indicative of transport distances generally not more than a few hundred metres, sub-rounded grains with minor mechanical deformation are indicative of moderate fluvial transport of 1-5 km and well-rounded, polished or extensively flattened grains are indicative of longer transport exceeding several kilometres (Chapman *et al*., 2021; Townley *et al*., 2003). The sub-rounded outlines and partially preserved internal textures reported here, as well as the preservation of delicate euhedral mineral inclusions in the Besenge 3 grains, suggest that the primary lode sources are within a proximal-to-moderate transport distance to both sampling localities. This also agrees with the moderate maturity of the placer grains: they exhibit signs of mechanical abrasion (pitting, surface cavities, minor edge rounding) but are not as flattened or as smooth-surfaced as well-travelled, mature placer gold.

These results are in good agreement with studies of gold grain morphology in structural and geological analogue Pan-African basement settings of Central and West Africa. (Central African Fold Belt) In northern Cameroon, Fuanya *et al*. (2019) described gold grains with irregular to rounded morphology and proximal-source microtextures within 5 km of the bedrock source, attributed to granitoids and schists with multiple quartz veins. Nguimatsia Dongmo *et al*. (2019) observed angular to sub-rounded gold grains with complex outlines, striations, pits and cavities in the Ako'ozam and Njabilobe districts of southwestern Cameroon. The authors inferred restricted transport distances based on the morphological parameters. On a local scale, investigation of alluvial gold from the Kushaka and Rafin Gora drainage systems of northwestern Nigeria (Omang, 2003) and from the Wonaka schist belt in the Nigerian Basement Complex showed irregular to sub-

rounded gold grain morphologies with grooves, pits and cavities filled with clays, all of which were interpreted as indicative of proximity to the primary lode source (directly comparable with the present study).

The core-rim Ag-depletion microtexture observed in the Oban 1 population of Grain 3 (core Ag = 6.33 wt.% versus rim Ag = 2.45 wt.%) is a feature of the supergene modification of placer gold during residence in tropical fluvial systems. Under supergene conditions, acidic, oxidizing groundwaters selectively leach Ag from gold alloys (Bowell *et al*., 1993), leaving Au-enriched, Ag-depleted rims that appear brighter in BSE images. This mechanism of self-electrorefining, by which Au complexes in solution reprecipitate as near-pure gold overgrowths on grain surfaces, has been experimentally demonstrated (Groen *et al*., 1990) and is widely reported in tropical placer gold systems. Kouankap *et al*. (2021) reported the presence of Ag-depleted rims in gold grains with a fineness up to 1000 from the Abiete-Toko Gold District of South Cameroon and attributed the rims to core-rim zonation resulting from supergene leaching during fluvial transport, as described for the Oban 1 observation. The Amani Placer Gold Deposit, Tanzania (Dunn & von der Heyden, 2021), provided compelling evidence of secondary Ag-depleted overgrowth rims approaching 100 wt.% Au, formed by de-alloying enhanced in lateritic, Cl-Fe-rich supergene environments. On a global scale, Ketchaya *et al*. (2024) reported the same core-rim Ag-depletion pattern in gold grains from the Nyema and Zingui placer deposits of southern Cameroon, which they attributed to chemical de-alloying and supergene biogeochemical redistribution of Au in a humid tropical setting similar to that of the Obudu-Oban Massif.

4.2.5 Significance of Mineral Inclusions

The sub-rounded cassiterite inclusion (O = 46.78 wt%, Sn = 53.22 wt%; total = 100.00 wt%) in the Oban 1 gold grain is stoichiometrically pure SnO2 and is consistent with primary cassiterite with minimal substitution of Fe, Ta, or Nb. Cassiterite is the main ore mineral of tin and occurs primarily in high-temperature hydrothermal veins (300-600 degrees C), granite pegmatites, and greisens associated with evolved peraluminous granites (Kinnaird, 2016).

Cassiterite is a dense mineral resistant to tropical weathering and thus tends to concentrate efficiently in alluvial placer deposits, usually within a few kilometres of the primary granitic source (Njiganga *et al*., 2023). The co-entrapment of cassiterite with gold in a single grain matrix provides direct mineralogical evidence that the primary gold-forming system in the Oban 1 catchment is a granite-related hydrothermal gold-tin system—most plausibly Sn-Au mineralization hosted in greisen-type quartz-cassiterite veins or tourmaline-bearing quartz veins associated with the evolved granitic intrusions of the Oban Massif documented by Oden (2012) and Ekwueme and Kroner (2006).

The presence of Sn-Au genetic coupling in the Oban Massif aligns with Nigeria's general metallogenetic framework, where minor tin-bearing pegmatites have been reported in the Obudu and Oban massifs of southeastern Nigeria (Kinnaird *et al*., 2016). Gold-tin associations linked to peraluminous granite-related systems are well established at the continental scale in Pan-African basement terrains across Africa, including the Kivu-Maniema tin fields of the Democratic Republic of Congo (Dewaele *et al*., 2015), the Karagwe-Ankole Belt of Rwanda and Uganda (Dewaele *et al*., 2015), and the Mesozoic anorogenic ring complexes of Nigeria, where greisenization produced cassiterite with associated Cu-Zn-Pb sulphides (Kinnaird *et al*., 2016). A regional proximal analogue occurs in the Tcholliré gold district of northern Cameroon. Gold and electrum grains were co-recovered with cassiterite from stream-sediment pan concentrates, confirming the association of

gold with Sn-bearing mineralization in Pan-African granitoid-metasediment settings (Ketchaya *et al*., 2024). The two euhedral monazite inclusions from Besenge 3 gold grains are Ce-dominant, with an approximate formula of (Ce, La, Nd, Pr, Sm), PO4 and a significant amount of Zr (5.07-6.04 wt.%).

Both inclusions are euhedral in habit, a feature that is especially diagnostic. Euhedral mineral inclusions in placer gold suggest that the host mineral phases crystallized during the same hydrothermal or metamorphic event as the gold and were subsequently trapped as solid inclusions during the precipitation of gold from ore-forming fluids at depth (Kouankap *et al*., 2021). The retention of euhedral shape within the gold matrix indicates minimal mechanical reworking of the encasing grain — consistent with the sub-rounded to moderately sub-rounded grain morphology and the inference of proximal transport.

Monazite chemistry is important for genetic interpretation. EMPA data indicate LREE-enriched compositions, with La_2O_3 + Ce_2O_3 comprising ~17-19 wt.% of the total, together with P (7.78-8.78 wt%), Nd (up to 4.47 wt%) and Zr (5.07-6.04 wt%). Importantly, Th is at or below the EMPA detection limit in both analyses. Studies of hydrothermal monazite chemistry in several gold deposit types have shown that hydrothermal monazite associated with orogenic gold mineralization is characterized by high total LREE (La2O3 + Ce2O3 > 51 wt%), low ThO_2 (< 1.5 wt.%) and distinctive Ce/Pr and La/Nd ratios, diagnostic values that differ from those of metamorphic monazite (lower LREE, higher Th) and magmatic monazite (Braize *et al*., 2026; McClenaghan, *et al*., 2019). The lack of detectable Th and the LREE-enriched nature of the Besenge 3 monazites are consistent with hydrothermal monazite associated with orogenic gold mineralization in metamorphic basement rocks, rather than primary magmatic monazite in granites or migmatites. This interpretation is supported by the regional metamorphic setting. The Obudu Plateau basement rocks consist of migmatitic gneisses, granulites, amphibolites, and charnockites that underwent Pan-African high-grade metamorphism at about 600 Ma (Ekwueme & Kroner, 2006), providing the thermal and structural framework for the co-precipitation of orogenic gold-monazite from metamorphic-hydrothermal fluids in shear zones.

Monazite inclusions in alluvial gold have been reported in comparable regional settings by Kouankap *et al*. (2021) in streams draining Pan-African migmatite-dominated catchments of the Meiganga area in Cameroon, where monazite, pyrite and apatite entombed in gold grains were interpreted as a "metamorphic overprint in a magmatic-hydrothermal system". Nguimatsia Dongmo *et al*. (2019) also identified monazite as a characteristic mineral associated with gold in southwestern Cameroon, attributed to a magmatic-metamorphic gold-forming environment consistent with Pan-African basement geology. The presence of euhedral monazite in Besenge 3 gold and the metamorphic composition of the Obudu Plateau basement strongly favour an orogenic metamorphic-hydrothermal gold system as the primary source for the Besenge 3 placer.

4.2.6 Effect of the gold fineness on the alloy composition and on the discrimination of the deposit type

Fineness at Oban 1 ranges from 936.19 to 1000.00, and the single grain shows a core-rim decrease from 936.19 to 975.21 (Table 8). This variation is likely due to multiple gold-deposition events by compositionally heterogeneous hydrothermal fluids in a granite-related source system, or to sampling grains from more than one gold-bearing structure in the catchment. A particularly diagnostic feature is the presence of minor Cu (up to 1.16 wt%) in both core and rim analyses. Cu in gold alloys is a reliable proxy for higher-temperature hydrothermal precipitation (approximately 300-500 degrees C), as Cu preferentially partitions

into gold under magmatic-hydrothermal conditions (Liu *et al*., 2024). Elevated Cu, cassiterite inclusions, and variable fineness fingerprinting identify the Oban 1 gold as derived from a high-temperature, granite-related hydrothermal (greisen or quartz-vein) Sn-Au system. This interpretation aligns with the overall geochemical signature of Sn-Au mineralization worldwide, where gold associated with cassiterite-bearing hydrothermal veins in granitic systems generally has moderate-to-high fineness with minor Cu (Liu *et al*., 2024).

The Besenge 3 gold is characterized by high and consistent fineness (990–996), low Ag (0.43–2.48 wt.%) and Cu (<1 wt.%), and a narrowly clustered Au–Ag alloy. This compositional signature is diagnostic of orogenic metamorphic-hydrothermal gold systems, in which low-salinity, CO2-rich metamorphic fluids at moderate temperatures (250-450 °C) precipitate gold that is consistently low in Ag and essentially devoid of Cu, Hg, or Bi (Groves *et al*., 2003). The fine-grained range indicates a single, fairly homogeneous primary gold source, most likely a structurally controlled quartz-vein system within the metamorphic basement of the Obudu Plateau. Similar fineness values (90-101% Au) for the Kushaka schist belt of northwestern Nigeria (Omang, 2023) are within the ranges reported in the present study and were attributed to proximity to the main source in a Pan-African metamorphic setting and to a narrow range of compositions and angular to subrounded grain morphology.

Fineness values from both localities (936-1000 at Oban 1; 990-996 at Besenge 3) are broadly consistent with placer gold from Pan-African and Precambrian basement terrains across Africa. Kouankap *et al*. (2021) found a gold fineness of 826-1000 in an essentially binary Au-Ag alloy from the Abiete-Toko Gold District of South Cameroon and interpreted the gold to be of orogenic origin. Fuanya *et al*. (2019) reported alluvial gold EMPA data from the Gamba district, northern Cameroon, suggesting hydrothermal-orogenic sources with mineral inclusions (silicates, oxides, phosphates) and Au-Ag alloy compositions consistent with magmatic-metamorphic gold formation. In the Meyos-Essabikoula area, southern Cameroon, Omang *et al*. (2025) reported gold grains from the Nyong River with 93.54-99.29 wt% Au (comparable to the Besenge 3 range), and proposed that they were derived from a single event of hydrothermal deposition of gold from low-Ag fluids. Ketchaya *et al*. (2024) observed near-pure Au rims (~99.9 wt%) atop Ag-rich cores in southern Cameroon (Nyema and Zingui), confirming the universality of supergene Ag depletion in equatorial African placer gold. Secondary gold deposits in tropical settings have very high fineness (995–1000) worldwide, due to intensive supergene Ag leaching, as exemplified by the Nilambur Valley placer gold in India (Santosh *et al*., 1992) and lateritic weathering profiles in Mali and West Africa (Freyssinet *et al*., 1989).

4.2.7 Genetic Models and Implications for Exploration

The combined EMPA evidence of mineral inclusions, gold-alloy microchemistry and grain microtexture allows us to formulate two different genetic models for the primary gold sources in the Obudu-Oban Massif.

The cassiterite inclusion, minor Cu content, and wide fineness range at Oban 1 together define a granite-related magmatic-hydrothermal gold-tin mineralization style. Gold was probably co-precipitated with cassiterite from Sn-bearing hydrothermal fluids (~300-500 degrees) associated with evolved peraluminous granitoid intrusions of the Oban Massif. This is consistent with the known occurrence of Sn-bearing pegmatites in the Obudu-Oban area (Kinnaird *et al*., 2016), the Nb-Sn PCA factor documented in this study, and Sn-Au systems in analogous Pan-African granitic belts in Africa and globally. This represents a new Sn-Au mineralization style in south-eastern Nigeria and extends the known distribution of

granite-related gold systems in the Nigerian Basement Complex.

The euhedral monazite inclusions with LREE-dominant, low-Th compositions, the consistently high but narrowly clustered fineness (990-996), and the absence of Cu at Besenge 3 point to an orogenic metamorphic-hydrothermal gold system as the primary source. Orogenic gold deposits are the world's most economically important type of gold deposit, accounting for >75% of global historical gold production (Groves *et al*., 2003). They are characterized by structurally controlled quartz-carbonate veins hosted within greenschist- to amphibolite-facies shear zones, with accessory phases of low-Ag, Cu-poor gold and hydrothermal monazite. The Pan-African tectonic framework of the Obudu Plateau is characterized by well-documented shear zones, structural complexity, and a high-grade metamorphic basement (Ekwueme & Kroner, 2006). This is exactly the structural and lithological setting predicted for orogenic gold mineralization. This discovery has major implications for exploration and identifies the Besenge catchments as priority targets for systematic prospecting for structurally controlled quartz-vein gold mineralization on the Obudu Plateau.

4.2.8 Statistical assessment of elemental associations, geochemical similarities, origin, source and evolution

The dominant component, PC1, defines a coherent Fe-Ti-Ni-Mn-P-Nb-Sn-Zr-Pt assemblage diagnostic of heavy-mineral placer concentrations derived from mafic-ultramafic and pegmatitic source rocks. The presence of Fe, Ti, Mn, and P indicate the presence of dense, chemically resistant phases such as ilmenite (FeTiO3), magnetite (Fe_3O_4), and apatite, which preferentially concentrate in fluvial placers. An identical Fe-Ti factor was identified by Steiner (2021) as the first component in west-central Nigeria and was attributed to scavenging by ilmenite and Fe-Mn oxide-hydroxides in stream sediments. The Nb (0.81) and Sn (0.72) loadings are consistent with coexisting columbite-tantalite and cassiterite, reflecting pegmatite-derived detritus previously reported by Adetona *et al*. (2025) in the Pan-African Mineral Belt of north-central Nigeria. The Pt loading (0.64) suggests native platinum in the heavy-mineral fraction, analogous to PGE-placer behaviour in Bushveld Complex catchments, South Africa (Junge *et al*., 2019), whereas the high P loading (0.91) indicates apatite and monazite concentration along with ilmenite – similar to Fe-P-Ti placer associations reported from Precambrian basement catchments, Ghana (Abu *et al*., 2019).

The most exploration-significant associations in the dataset include PC2 loadings for Ce (0.97), Y (0.94), Pd (0.92), Nd (0.69), Dy (0.77), Zr (0.75), Si (0.60), and Au (0.49). The Ce-Y-Nd-Dy suite comprises resistant REE minerals (monazite, xenotime, and allanite) derived from the granitic-gneissic basement, while Zr is carried by zircon as an HFSE. Both groups align with the HFSE-REE factor identified by Lapworth *et al*. (2012) in west-central Nigeria and assigned to REE-pegmatite intrusion. The geochemically conspicuous co-loading of Pd (0.92) with REEs most plausibly reflects co-deposition of Pd-sulphides and REE minerals from related hydrothermal fluids. Similar Au-Pd-REE co-clustering has been reported in the stream sediments of the Betare-Oya gold district in Cameroon (Ateh *et al*., 2026). The Si-Zr matrix is consistent with quartz-hosted REE-PGE veins or NYF pegmatites described from the Eastern Desert of Egypt (Ibrahim, 2021) and the Manjo area of Cameroon (Fomekong *et al*., 2026).

PC3 is characterised by Na (0.97), Co (0.95), Cu (0.93), Ca (0.84), Mg (0.82), Al (0.76), and Sr (0.55), indicating a mafic-to-intermediate igneous provenance. The Na-Ca-Sr-Al suite is a classic fingerprint of plagioclase feldspar, whereas Mg, Co, and Cu reflect inputs from ferromagnesian minerals (pyroxene, amphibole, biotite) in gabbroic

and amphibolitic source rocks. High Na at UTK (2.95 %), OB 4 (7.00 %), and BSE 1 (3.17 %) corresponds to catchments draining plagioclase-rich granitoids of the Oban Massif (Oden, 2012). This factor is similar to the mafic provenance components reported in the Tanzania Craton (Kasanzu 2025) and in coastal creeks of southwestern Nigeria, where tropical weathering occurs. High Cu loading suggests that Cu-bearing mafic intrusions or amphibolitic units within the Massif may be targets for disseminated copper mineralisation, as noted for analogous V-Ni-Fe-Cu-Co factors in the Tchangue-Bikoui drainage of southern Cameroon (Nforba *et al*., 2020).

PC4 is characterized by Cr (0.82), La (0.82), Ba (0.80), Rh (0.74), Se (0.66) and Re (0.51). The Cr-Rh coupling is diagnostic of chromite-bearing ultramafic lithologies, as Rh (an IPGE) partitions strongly into chromite spinel – analogous to Cr-Rh-Pd associations used as chromitite proximity markers in Bushveld Complex catchments (Junge *et al*., 2015) and perhaps associated with metaperidotites on the Obudu Plateau (Ekwueme & Kroner, 2006). Co-loading of La with Cr likely reflects secondary LREE enrichment by metasomatic fluids associated with chromite alteration, as documented in REE-bearing veins cutting serpentinites in the Arabian-Nubian Shield (Ibrahim, 2021). The Ba loading (0.80) indicates barite vein mineralization in fault zones at the Obudu–Oban basement–Cretaceous sediment boundary (Ekwueme *et al*., 2015), consistent with hydrothermal Ba anomalies reported in the Onyami River drainage, southwestern Nigeria (Adepoju, 2019).

PC5 defines a Tb (0.93)-Sm (0.89)-Ir (0.68)-Pt (0.60)-Fe (0.56) association, which reflects MREE-HREE fractionation that occurs alongside iridium-group PGEs. Tb and Sm are enriched in garnet and amphibole in the metamorphic basement (Ekwueme & Kroner, 2006). Ir and Pt are indicative of PGE enrichment in magmatic sulphide phases in mafic-ultramafic intrusions. Their co-association with Fe and MREE indicates that sulphide-rich zones in mafic bodies may be PGE targets, with MREE enrichment in adjacent metamorphic aureoles. Similar Pt-Pd-Au-mafic element clustering in stream sediments has been observed in As-Mo-W sulphide mineralisation factors from northern Cameroon (Embui *et al*., 2024).

PC6 is dominated by Sb (0.97), Rb (0.83), K (0.69), and Pb (0.69), which is a classic epithermal-to-mesothermal hydrothermal signature. Sb is the most reliable gold pathfinder in both epithermal and orogenic systems globally, as stibnite or tetrahedrite in Au-quartz veins. Zoheir, *et al*. (2020) reported the As-Sb-Hg pathfinder suite for gold in Pan-African terrains of the Egyptian Eastern Desert. The Rb-K co-loading indicates sericitic or potassic wall-rock alteration typical of orogenic gold systems, consistent with K-Rb-Pb hydrothermal alteration factors in the Onyami drainage (Adepoju, 2019) and the Kaiama gold district (Alepa *et al*., 2019) of the Nigerian Basement Complex. The high Sb loading justifies priority follow-up sampling along the Besenge-Oban corridor.

As (0.72) dominates PC7, with negative loadings on V (-0.61) and Eu (-0.71). As is the most globally consistent gold pathfinder in orogenic systems, occurring as arsenopyrite in metamorphic basement shear zones (Meng *et al*., 2023). The separation from Sb (PC6) shows a bi-modal As-Sb gold pathfinder structure, consistent with multi-stage orogenic gold mineralization, involving early arsenopyrite precipitation and later stibnite deposition (Groves *et al*., 2013). The negative Eu loading (-0.71) indicates feldspar-controlled Eu2+ depletion during Pan-African granitic differentiation, as reported for granites and migmatites of the Obudu area (Ibe & Obiora, 2019). The inverse V-As relationship indicates that As is enriched in reducing, sulphide-dominated hydrothermal environments where V is locally depleted.

PC8 (Er = 0.89, Ru = 0.81, Cd = 0.81, Ho = 0.70) represents HREE placer mineralization (Er, Ho in xenotime and zircon) associated with Ru (a PGE present in laurite, RuS2) and Cd, the latter likely derived from sphalerite detritus. Similar co-concentrations of HREE-PGE placers have been reported in the Betare-Oya district of Cameroon (Ngatcha *et al*., 2025). PC9 (Os=0.83, Re=0.78) separates a mantle-derived siderophile PGE signature, distinct from the chalcophile Pd-Au enrichment of PC2 and the Ir-Pt sulphide signal of PC5. The separation of Os-Re into a distinct phase suggests an opportunity to use a geochemical indicator of primitive mafic intrusions, which may be amenable to Re-Os isotopic dating (Naldrett, 2004), in the Obudu-Oban Massif.

PC10 is characterised by a strong negative Pr loading (-0.87), indicative of independent fractionation of praseodymium, probably due to selective retention in monazite or rhabdophane relative to allanite. PC11 (Gd = 0.61, Nd = 0.50) represents the residual MREE variance associated with garnet-controlled fractionation in the metamorphic basement (Ekwueme & Kroner, 2006). Together, they explain only 4.6% of the variance individually but are geochemically interpretable.

The 11-component PCA model reveals four major geochemical processes: (i) heavy mineral placer concentration of Fe-Ti oxides, Nb-Sn resistates and PGE alloys (PC1, PC8); (ii) REE-HFSE enrichment from pegmatitic and hydrothermal sources co-associated with Pd-Au (PC2, PC10, PC11); (iii) mafic/calc-silicate provenance and plagioclase weathering (PC3, PC4); and (iv) multi-stage hydrothermal mineralisation expressed through Sb-Rb-K-Pb (PC6), As (PC7) and sulphide-PGE pathfinder suites (PC5, PC9). This multi-process framework is consistent with the known geological architecture of the Obudu-Oban Massif and is analogous to PCA frameworks established for similar Pan-African terrains.

4.0 Conclusion

This study integrated ICP–MS geochemistry, multivariate statistical analysis, SEM–EDS mineral characterization, XRD mineralogical investigations, and EMPA gold-grain microchemistry to evaluate the origin and metallogenic evolution of mineralization in the Obudu Plateau–Boki–Oban Massif of southeastern Nigeria. The combined dataset provides compelling evidence that the study area hosts a complex mineralizing system formed by multiple tectono-magmatic and hydrothermal processes associated with the Pan-African Orogeny.

Geochemical investigations revealed significant enrichment of Au, As, Sb, Pb, Sn, Nb, Y, and rare-earth elements, indicating the presence of both hydrothermal gold and rare-metal mineralization systems. Principal Component Analysis successfully distinguished ore-related geochemical associations and identified Au–As–Sb and Nb–Sn–REE assemblages as the dominant mineralization signatures. Tectonic discrimination diagrams further suggest that the mineralized rocks evolved within convergent-margin environments characterised by volcanic-arc magmatism, syn-collisional granitoid emplacement, and subsequent crustal reworking, thereby providing favourable conditions for hydrothermal fluid circulation and metal concentration.

Gold-grain morphology and microtexture indicate relatively short transport distances from the primary source, with the preservation of sub-rounded grain morphologies, core–rim zonation, and delicate mineral inclusions supporting derivation from proximal mineralized bedrock sources. Gold fineness values of 936–1000 in Oban and 990–996 in Besenge, together with characteristic Ag-depletion rims, reflect both primary alloy chemistry and subsequent supergene modification.

Mineral inclusion studies provide the strongest evidence for contrasting mineralization styles across the study area. Cassiterite inclusions within Oban gold

grains, accompanied by minor Cu enrichment and variable fineness, indicate precipitation from high-temperature Sn-bearing hydrothermal fluids associated with evolved granitoids and pegmatitic systems of the Oban Massif. Conversely, euhedral monazite inclusions within Besenge gold grains, characterized by LREE enrichment and negligible thorium, indicate hydrothermal monazite formation during structurally controlled metamorphic-hydrothermal gold mineralization in the Obudu Plateau.

Integrated evidence demonstrates the coexistence of two genetically distinct yet spatially related metallogenic systems within the Obudu–Oban basement province. The Oban Massif hosts granite-related magmatic-hydrothermal Au–Sn mineralization associated with evolved peraluminous granitoids, whereas the Obudu Plateau is dominated by orogenic, metamorphic-hydrothermal gold mineralization localized within Pan-African shear-zone networks. Subsequent tropical weathering and fluvial reworking liberated gold and associated heavy minerals into modern drainage systems, producing the placer occurrences identified in this study.

The study therefore presents the first integrated metallogenic model for the Obudu Plateau–Boki–Oban Massif, significantly advancing understanding of mineralization processes in southeastern Nigeria. From an exploration perspective, the Besenge–Obudu corridor is a highly prospective target for structurally controlled quartz-vein-hosted orogenic gold deposits, whereas the Oban Massif is an emerging Au–Sn–Nb–REE province where exploration should focus on greisenized granites, pegmatites, and quartz–cassiterite vein systems. Recognizing these dual metallogenic systems substantially enhances the mineral prospectivity of southeastern Nigeria and provides a robust framework for future mineral exploration and resource development.

5.0 References

Abu, M., Sunkari, E. D., & Şener, M. (2019). Untapped economic resource potential of the Neoproterozoic to Early Paleozoic Volta Basin, Ghana: A review. *Natural Resources Research, 28*(4), 1429–1445.

Adepoju, M. O. (2019). Geochemical soil survey for base and precious metals in Dagbala-Atte District, southwestern Nigeria. *International Journal of Geosciences, 10*(2), 141–159.

Adetona, A. A., Salako, K. A., Olarionye, O., Alabi, A. A., Rafiu, A. A., & Alhassan, U. D. (2025). Geo-investigation for gold mineralisation veins in part of Kushaka Schist Belt, Niger State, Nigeria, using an integrated approach. *FUDMA Journal of Renewable and Atomic Energy, 2*(1), 85–105.

Alepa, V. C., Bale, R. B., Alimi, S. A., & Bonde, D. S. (2019). Reconnaissance geochemical exploration in Kaiama, North Central Nigeria. *Saudi Journal of Engineering and Technology, 4*(11), 457–472.

Asaah, A. V., Zoheir, B., Lehmann, B., Frei, D., Burgess, R., & Suh, C. E. (2015). Geochemistry and geochronology of the ~620 Ma gold-associated Batouri granitoids, Cameroon. *International Geology Review, 57*(11–12), 1485–1509.

Ateh, K. I., Ngatcha, B. R., Tata, E., Vishiti, A., Chombong, N. N., Kwanyang, L. T., et al. (2026). Quartz vein characteristics and pyrite-hosted invisible gold microchemistry from the Bétaré Oya Gold District, Lom Basin, Eastern Cameroon. *Journal of the Cameroon Academy of Sciences, 22*(3), 263–284.

Barnes, S. J., & Lightfoot, P. C. (2005). *Formation of magmatic nickel sulfide deposits and processes affecting their copper and platinum group element contents.* GeoScienceWorld, https://doi.org/10.5382/AV100.08

Benkhelil, J. (1982). Benue trough and Benue chain. *Geological Magazine, 119*(2), 155–168.

Bowell, R. J., Foster, R. P., & Gize, A. P. (1993). The mobility of gold in tropical rainforest soils. *Economic Geology, 88*(5), 999–1016.

Braize, D., Steadman, J. A., Meffre, S., & Farias, P. (2026). Insights on the formation of the Warrego Au–Cu–Bi deposit from monazite and xenotime U–Pb dating: A new mineralization event in the Tennant Creek Province. *Precambrian Research, 442*, 108149.

Chapman, R. J., Banks, D. A., Styles, M. T., Walshaw, R. D., Piazolo, S., Morgan, D. J., et al. (2021). Chemical and physical heterogeneity within native gold: Implications for the design of gold particle studies. *Mineralium Deposita, 56*(8), 1563–1588.

Chapman, R. J., Mortensen, J. K., & LeBarge, W. P. (2010). Application of microchemical characterization of placer gold grains to exploration. *Economic Geology*.

Chukwu, A., & Obiora, S. C. (2021). Petrogenetic characterization of pegmatites and their host rocks in southern Akwanga, North-Central Basement Complex, Nigeria. *Journal of Earth System Science, 130*(1), 18, https://doi.org/10.1007/s12040-020-01498-7

Cullity, B. D., & Stock, S. R. (2001). *Elements of X-ray diffraction*. Prentice-Hall.

Dada, S. S., Olobaniyi, S. B., Oha, I. A., Goki, N. G., Salawu, N. B., Ibe, C. U., & Garba, A. A. (2024). Crustal evolution and the Nigerian metallogenic framework. In *Geology and natural resources of Nigeria* (pp. 200–222). CRC Press.

Dewaele, S., Muchez, P., Burgess, R., & Boyce, A. (2015). Geological setting and timing of cassiterite-vein-type mineralization in the Kalima area (DRC). *Journal of African Earth Sciences, 112*, 199–212.

Dongmo, F. W. N., Chapman, R. J., Bolarinwa, A. T., Yongue, R. F., Banks, D. A., & Olajide-Kayode, J. O. (2019). Microchemical characterization of placer gold grains from southern Cameroon. *Journal of African Earth Sciences, 151*, 189–201.

Dunn, S. C., & von der Heyden, B. P. (2021). Gold remobilization in gossans of the Amani area, Tanzania. *Ore Geology Reviews, 131*, 104033.

Ekwueme, B. N. (2003). *The Precambrian geology and evolution of the Southeastern Nigerian Basement Complex*. University of Calabar Press.

Ekwueme, B. N., & Kröner, A. (2006). Zircon ages of Obudu Plateau granulites. *Journal of African Earth Sciences, 44*(4–5), 459–469.

Ekwueme, B. N., Akpeke, G. B., & Ephraim, B. E. (2015). Barite mineralization in southeastern Nigeria. *Global Journal of Geological Sciences, 13*, 53–66.

Embui, V. F., Mbafor, P. U., Teh, A. N. A., & Moudioh, C.-A.-M. M. (2024). A review of granite melt source, and associated gold fertility potential in Batouri, Betare Oya, Meiganga, and Ngazi-Tina gold districts in the eastern goldfield of Cameroon: Insight from zircon chemistry. *Ore and Energy Resource Geology*, *17*, Article 100067. https://doi.org/10.1016/j.oreoa.2024.100067

Ene, E., Okonkwo, I., & Udosen, E. (2021). Structural control of gold mineralization in southeastern Nigeria. *Journal of African Earth Sciences, 180*, 104253, https://doi.org/10.1016/j.jappgeo.2023.104969

Feybesse, J. L., Billa, M., Guerrot, C., et al. (2006). Geodynamic model of the Ghanaian province. *Precambrian Research, 149*(3–4), 149–196.

Fomekong, B. K., Kouankap Nono, G. D., Afahnwie, N. A., Ngong, G. Y., Fontem, N. B., Yiika, L. P., & Wotchoko, P. (2026). Geochemistry of alluvial sediments from the Bipindi–Kouambo prospect (Cameroon): Provenance,

depositional environment and mineralization potential. *Arabian Journal of Geosciences*, *19*(6), Article 111. https://doi.org/10.1007/s12517-026-12508-1

Freyssinet, P., Zeegers, H., & Tardy, Y. (1989). Gold grains in lateritic profiles. *Journal of Geochemical Exploration, 32*(1–3), 17–31.

Fuanya, C., Bolarinwa, A. T., Kankeu, B., Yongue, R. F., Tangko, E. T., & Nkepguep, F. Y. (2019). Geochemical characteristics and petrogenesis of basic rocks in the Ako'ozam–Njabilobe area, Southwestern Cameroon: Implications for Au genesis. *SN Applied Sciences*, *1*, Article 904. https://doi.org/10.1007/s42452-019-0959-5

Goldfarb, R. J., & Groves, D. I. (2015). Orogenic gold deposits. *Lithos*.

Goldstein, R. H. (2003). Petrographic analysis of fluid inclusions.

Groen, J. C., Craig, J. R., & Rimstidt, J. D. (1990). Gold-rich rim formation on electrum grains. *The Canadian Mineralogist, 28*(2), 207–228.

Groves, D. I., Goldfarb, R. J., Gebre-Mariam, M., et al. (1998). Orogenic gold deposits classification. *Ore Geology Reviews, 13*(1–5), 7–27.

Groves, D. I., Goldfarb, R. J., Robert, F., & Hart, C. J. (2003). Gold deposits in metamorphic belts. *Economic Geology, 98*(1), 1–29.

Harbi, H. M. (2019). U–Pb zircon geochronology of Afif Terrane plutonic rocks. In *Arabian Plate and surroundings* (pp. 161–190). Springer.

Haruna, I. V. (2017). Geochemistry of Pan-African granitoids in Nigeria. *Geoscience Frontiers, 8*(5), 1255–1274.

Hilson, G. (2002). Small-scale mining impacts. *Natural Resources Forum, 26*(1), 3–13.

Ibe, C. U., & Obiora, S. C. (2019). Granitoid geochemistry in Nigeria. *Acta Geochimica, 38*(5), 734–752.

Ibrahim, W. S. (2021). Pegmatites in South Eastern Desert, Egypt. *Acta Geologica Sinica, 95*(6), 2045–2062.

Jarvis, I. (1992). Sedimentology of phosphatic chalks. *Sedimentology, 39*(1), 55–97.

Johnson, P. R. (2021). Arabian–Nubian Shield geology. In *The geology of the Arabian-Nubian Shield* (pp. 1–38). Springer.

Junge, M., Oberthür, T., Kraemer, D., et al. (2019). Platinum-group elements in Bushveld Complex ores. *Mineralium Deposita, 54*(6), 885–912.

Junge, M., Wirth, R., Oberthür, T., et al. (2015). PGE distribution in pentlandite. *Mineralium Deposita, 50*(1), 41–54.

Kasanzu, C. H. (2025). Geochemistry of Rukwa Basin sediments. *Journal of Sedimentary Environments, 10*(3), 635–648.

Ketchaya, Y. B., Zhou, T., Santosh, M., et al. (2024). Supergene gold transformations in Cameroon. *Ore Geology Reviews, 166*, 105948.

Kinnaird, J. A. (1985). Hydrothermal alteration in Nigerian ring complexes. *Journal of African Earth Sciences, 3*(1–2), 229–251.

Kinnaird, J. A., Nex, P. A., & Milani, L. (2016). Tin in Africa. *Episodes, 39*(2), 361–380.

Kouankap, D., Bongsiysi, F. F. E., Tamfuh, P. A., Jacob, A., Nyangono Abolo, A. J., Fomekong, B. K., Kibong, N. F., & Suh, C. E. (2021). Gold deposit type and implication for exploration in the Abiete-Toko Gold District, South Cameroon: Constraint from morphology and microchemistry of alluvial gold grains. *Heliyon*, *7*(4), Article e06758. https://doi.org/10.1016/j.heliyon.2021.e06758

Liu, Z.-J., Yang, L.-Q., Xie, D., Yang, W., Li, D.-P., Feng, T., & Deng, J. (2024). Hydrothermal Alteration Processes of Xincheng Gold Deposit Jiaodong Peninsula, China: Constraints from

Composition of Hydrothermal Rutile. *Minerals*, *14*(4), 417. https://doi.org/10.3390/min14040417

McClenaghan, M. B. (2005). Indicator mineral exploration methods. *Geochemistry: Exploration, Environment, Analysis, 5*(3), 233–245.

McClenaghan, M. B., Paulen, R. C., & Kjarsgaard, I. M. (2019). Rare metal indicator minerals. *Canadian Journal of Earth Sciences, 56*(8), 857–869.

Meng, W., Liu, J., Wu, H., et al. (2023). Carlin-type gold deposit mechanisms. *Minerals, 13*(11), 1459.

Nforba, M. T., Egbenchung, K. A., Berinyuy, N. L., et al. (2020). Stream sediment geochemistry in Cameroon. *Geol Ecol Landsc.*

Ngatcha, R. B., Afahnwie, N. A., Etutu, M. E. M., et al. (2025). Stream sediment geochemistry in Cameroon. *Ore and Energy Resource Geology, 19*, 100104.

Njiganga, N. M., Tebogo, T. K., Ngatcha, R. B., Suh, C. E., Ilouga, D. C., Shemang, E. M., Tantoh, B. S., Tata, E., & Agyingi, C. M. (2023). Compositional provenance study of alluvial cassiterite at Bambol and Mayo Seni localities of the Mayo Darlé massif, northern Cameroon. *Journal of Sedimentary Environments*, *8*, 281–297. https://doi.org/10.1007/s43217-023-00136-8

Nzenti, J. P., Kapajika, B., Wörner, G., & Lubala, T. R. (2006). Pan-African granitoids in Cameroon. *Journal of African Earth Sciences, 45*(1), 74–86.

Oden, M. I. (2012). Pegmatite veins in Oban Massif. *Research Journal of Environmental and Earth Sciences, 4*(4), 381–389.

Okonkwo, I. O., & Folorunso, I. O. (2019). Shear zone-hosted gold mineralization in Nigeria. *Natural Resources Research, 28*(4), 1111–1128.

Okonkwo, I., Ekwueme, B., & Ocan, O. (2016). Pegmatite mineralization in Obudu Plateau. *Nigerian Journal of Mining and Geology, 52*(1), 53–65.

Olade, M. A. (2021). *Mineral deposits and exploration potential of Nigeria*. Prescott Books.

Omang, B. O. (2023). Stream sediment geochemistry in Nigeria. *Communication in Physical Sciences, 9*(3), 230–255.

Omang, O., Effiom, H., Omeka, E., et al. (2023). Soil geochemistry and health risk assessment. *Global Journal of Geological Sciences, 21*(1), 91–115.

Omang, B. O., Lohmeier, S., Vishiti, A., et al. (2025). Microchemical composition of alluvial gold. *Journal of Geosciences, 70*(4), 211.

Pirajno, F., & Goldfarb, R. J. (2017). Orogenic gold and exploration models.

Richards, J. P. (2022). Porphyry copper deposits. *Geosphere, 18*(1), 130–155.

Rollinson, H. (2014). Plagiogranites from the mantle section of the Oman Ophiolite: Models for early crustal evolution. *Geological Society, London, Special Publications*, *392*(1), 247–261. https://doi.org/10.1144/sp392.13

Rollinson, H. R. (1993). Limpopo Belt terrane interpretation. *Geological Magazine, 130*(6), 755–765.

Santosh, M., Philip, R., Jacob, M. K., & Omana, P. K. (1992). Placer gold formation in India. *Mineralium Deposita, 27*(4), 336–339.

Steiner, B. (2021). Stream sediment geochemistry tools. University of Exeter.

Tack, L., & Bowden, P. (1999). Post-collisional granites in Namibia. *Journal of African Earth Sciences, 28*(3), 653–674.

Toteu, S. F., Penaye, J., & Djomani, Y. P. (2004). Pan-African belt evolution. *Canadian Journal of Earth Sciences, 41*(1), 73–85.

Townley, B. K., Hérail, G., Maksaev, V., et al. (2003). Gold grain morphology in exploration. *Geochemistry: Exploration, Environment, Analysis, 3*(1), 29–38.

Whalen, J. B., Currie, K. L., & Chappell, B. W. (1987). A-type granites.

Contributions to Mineralogy and Petrology, 95(4), 407–419.

Wright, J.B., Hastings, D.A., Jones, W.B. and Williams, H.R. (1985) *Geology and Mineral Resources of West Africa*. George Allen and Unwin, London.

Zoheir, B., Goldfarb, R., Holzheid, A., et al. (2020). Um Rus granite and gold deposit geochemistry. *Geoscience Frontiers, 11*(1), 325–345.

Declarations

Ethical Approval and Consent to Participate

This study did not involve human participants, human tissues, or live animals. Therefore, ethical approval and consent to participate were not required.

Consent for Publication

Not applicable.

Funding

The authors received no financial support for the research, authorship, and/or publication of this article.

Availability of Data and Materials

All data generated or analyzed during this study are included in this published article. Additional information may be made available by the corresponding author upon reasonable request.

Competing Interests

The authors declare that they have no known competing financial interests or personal relationships that could have appeared to influence the work reported in this paper.

Acknowledgements

The authors gratefully acknowledge the support provided by colleagues and laboratory staff who assisted during field sampling, laboratory analyses, and manuscript preparation. The authors also appreciate the constructive comments of anonymous reviewers, which helped improve the quality of the manuscript.

Authors' Contributions

OAA contributed to the conceptualization of the study, methodology development, investigation, formal data analysis, and preparation of the original manuscript draft. BOO contributed to methodology, supervision, manuscript review, and editing. VA contributed to methodology, supervision, manuscript review, and editing. MEO contributed to data validation, manuscript writing, review, and editing. All authors read, reviewed, and approved the final manuscript and agree to be accountable for all aspects of the work.